AD-A093 423 AERONAUTICAL RESEARCH INST OF SWEDEN STOCKHOLM F/G 20/4
INVESTIGATION OF MODELING CONCEPTS FOR PLUME-AFTERBODY FLOW INT--ETC(U)
FEB 80 S E NYBERG, J AGRELL, T HEVRENG DA-ERO-78-G-028

UNCLASSIFIED NL

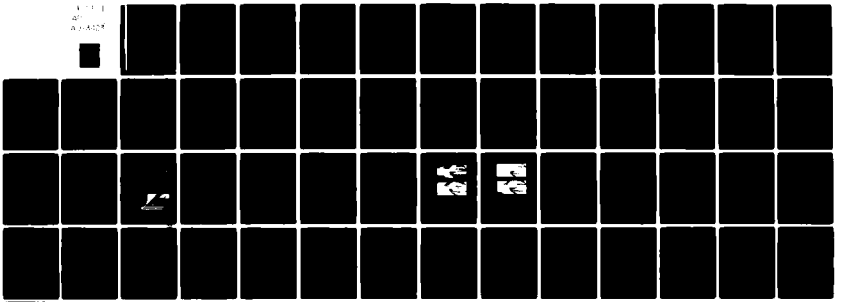

END
DATE FILMED
1-81
DTIC

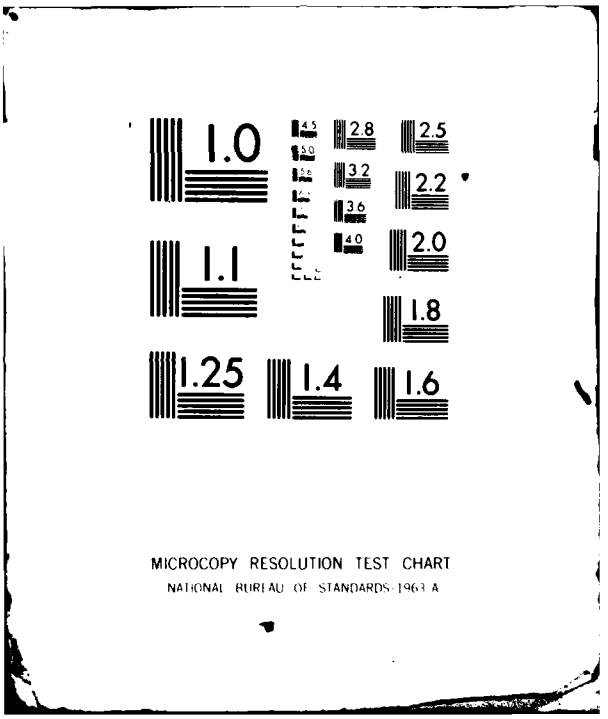
1.0
1.1
1.25
1.4
1.6
1.8
2.0
2.2
2.5
2.8
3.2
3.6
4.0
4.5
5.0
MICROCOPY RESOLUTION TEST CHART
NATIONAL BUREAU OF STANDARDS-1963 A

INVESTIGATION OF MODELING CONCEPTS FOR PLUME-AFTERBODY FLOW INTERACTIONS

2nd Annual Technical Report

by

S.-E. Nyberg
J. Agrell
T. Hevreng

February 1980

EUROPEAN RESEARCH OFFICE
United States Army
London England

GRANT NUMBER DA-ERO-78-G-028

Grantee: Georg Drougge, Dr., Deputy Director
THE AERONAUTICAL RESEARCH INSTITUTE OF SWEDEN (FFA)
Box 11021, S - 161 11 BROMMA, Sweden

Approved for Public Release; distribution unlimited

This research has been sponsored jointly by the US Army European Research Office and by the FFA.

UNCLASSIFIED

SECURITY CLASSIFICATION OF THIS PAGE (When Data Entered)

R&D 2515

REPORT DOCUMENTATION PAGE

READ INSTRUCTIONS BEFORE COMPLETING FORM

1. REPORT NUMBER

2. GOVT ACCESSION NO. AD-A093 423

3. RECIPIENT'S CATALOG NUMBER

4. TITLE (and Subtitle)

Investigation of Modeling Concepts for Plume-Afterbody Flow Interactions,

5. TYPE OF REPORT & PERIOD COVERED

2nd Annual Technical Report, No. 2

January 78 — March 80

6. PERFORMING ORG. REPORT NUMBER

7. AUTHOR(s)

S.E. Nyberg T. Hevreng
J. Agrell

8. CONTRACT OR GRANT NUMBER(s)

DA-ERO-78-G-028 NEW

9. PERFORMING ORGANIZATION NAME AND ADDRESS

The Aeronautical Research Institute of Sweden
(FFA)
Bromma, Sweden

10. PROGRAM ELEMENT, PROJECT, TASK AREA & WORK UNIT NUMBERS

1T161102BH57-06

11. CONTROLLING OFFICE NAME AND ADDRESS

USARDSG-UK
Box 65
FPO NY 09510

12. REPORT DATE

February 1980

13. NUMBER OF PAGES

54

14. MONITORING AGENCY NAME & ADDRESS (if different from Controlling Office)

15. SECURITY CLASS. (of this report)

Unclassified

15a. DECLASSIFICATION/DOWNGRADING SCHEDULE

16. DISTRIBUTION STATEMENT (of this Report)

Approved for Public Release; distribution unlimited

17. DISTRIBUTION STATEMENT (of the abstract entered in Block 20, if different from Report)

18. SUPPLEMENTARY NOTES

19. KEY WORDS (Continue on reverse side if necessary and identify by block number)

Plume Modeling

20. ABSTRACT (Continue on reverse side if necessary and identify by block number)

A high pressure hot gas supply system has been developed for the FFA 0.5 x 0.5 m S5 supersonic wind tunnel to allow the study of aerodynamic interference effects caused by plume induced flow separation on afterbodies. Capable of operating with gases covering a wide range of specific heat ratios, the facility serves to critically evaluate the merits and limitations of plume modeling techniques.

DD FORM 1 JAN 73 1473 EDITION OF 1 NOV 65 IS OBSOLETE

UNCLASSIFIED

SECURITY CLASSIFICATION OF THIS PAGE (When Data Entered)

20. Contd.

The facility is now fully operational. Plume modeling experiments have been performed using air and Freon-22 for jet simulation at a free stream Mach number of 2.0 and zero angle of attack. One prototype air nozzle and two Freon nozzles modeled in accordance with the methodology suggested by Korst have been investigated.

The Freon plume shapes have been found to be in close agreement with those of the corresponding air tests supporting the suggested modeling methodology and design procedures. The agreement between prototype and model base pressures was satisfactory not only for the design point but also for a rather wide range of off-design conditions. The more sensitive parameter, the location of the separation line on the conical afterbody, was equally well correlated but for a narrower range in the vicinity of the design point and only for the nozzle designed with the assumption of a weak shock closure condition.

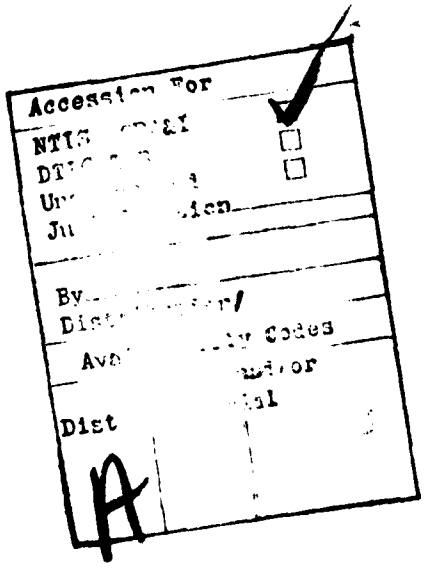

INVESTIGATION OF MODELING CONCEPTS FOR PLUME-AFTERBODY FLOW INTERACTIONS

2nd Annual Technical Report

S.-E. Nyberg
J. Agrell
T. Hevreng

SUMMARY

A high pressure hot gas supply system has been developed for the FFA 0.5 × 0.5 m S5 supersonic wind tunnel to allow the study of aerodynamic interference effects caused by plume induced flow separation on afterbodies. Capable of operating with gases covering a wide range of specific heat ratios, the facility serves to critically evaluate the merits and limitations of plume modeling techniques. The project, which is carried out in close cooperation with members of the Gas Dynamics Laboratory at the University of Illinois at Urbana-Champaign, is granted as a three year program.

During 1979, which is the second year of the program, the final shake down and calibration testing of the facility has been accomplished and the facility is now fully operational. Plume modeling experiments have been performed using air and Freon-22 for jet simulation at a free stream Mach number of 2.0 and zero angle of attack. One prototype air nozzle and two Freon nozzles modeled in accordance with the methodology suggested by Korst have been investigated.

The Freon plume shapes have been found to be in close agreement with those of the corresponding air tests supporting the suggested modeling methodology and design procedures. The agreement between prototype and model base pressures was satisfactory not only for the design point but also for a rather wide range of off-design conditions. The more sensitive parameter, the location of the separation line on the conical afterbody, was equally well correlated but for a narrower range in the vicinity of the design point and only for the nozzle designed with the assumption of a weak shock closure condition.

LIST OF CONTENTS

		Page
	SUMMARY	1
	NOMENCLATURE	5
1.	INTRODUCTION	7
2.	SIMULATION TEST FACILITY	9
	2.1 Introduction	9
	2.2 Systems performance tests	9
3.	REVIEW OF THE PLUME MODELING METHODOLOGY SUGGESTED BY KORST	12
4.	EXPERIMENTAL PROGRAM	16
	4.1 Wind tunnel models	16
	4.2 Calibration tests	17
	4.3 Plume modeling experiments	18
5.	CONCLUSIONS	21
	REFERENCES	22
	ACKNOWLEDGEMENT	24
	FIGURES	25
	APPENDIX	43
	Tables of recorded pressure	44-54

NOMENCLATURE

Geometry

	Afterbody
D	Forebody diameter [m]
L	Boattail length [m]
α	Angle of attack [deg.]
β	Boattail angle [deg.]
	Nozzle
R_L	Exit or lip radius [m]
θ_L	Conical divergence angle [deg.]

Tunnel Flow

P_{oE}	Stagnation pressure [Pa]
P_E	Freestream static pressure [Pa]
M_E	Freestream Mach No. [-]

Nozzle Flow

M_L	Lip Mach No. [-]*)
P_{oI}	Nozzle stagnation pressure [Pa]
P_L	Lip pressure [Pa]
T_{oI}	Nozzle stagnation temperature [^oC]
γ	Specific heat ratio [-]
ω_L	Prandtl-Meyer angle corresponding to M_L [deg.]

Plume

M_F	Surface Mach No. [-]
υ_F	Initial surface slope [deg.]
R_C	Initial surface curvature [m]
r_C	R_C/R_L [-]
ω_F	Prandtl-Meyer angle corresponding to M_F [deg.]

*) Conical source flow assumed, otherwise nozzle geometry and lip conditions have to be specified in greater detail, see Reference 16

Wake Conditions

s, S	Separation distance measured from end of boattail [m]
p_b, P_b, P_B	Base pressure [Pa]

SUBSCRIPTS

M	Model
P	Prototype
A	Air
F	Freon

1. INTRODUCTION

The interaction of rocket or jet plumes with the external flow over a vehicle as well as surrounding equipment or surfaces is important to system performance [1].*) In particular, such interactions are critical in their effects on the near wake base temperature and pressure, flow over the vehicle itself due to external flow separation, wake flow field at angle of attack, afterbody fin effectiveness, and launch equipment performance. Thus, the jet-slipstream interaction can give rise to undesirable aerodynamic performance by introducing drag penalties through lower than ambient pressures or, as the ratio of jet stagnation pressure to ambient pressure increases, by leading to plume induced separation [2]. In extreme cases, plume induced separation can result in catastrophic pitch up of missiles because of loss of stability or degradation of control effectiveness [3].

Rocket or jet plumes have been treated in wind tunnel tests using a variety of methods which include the use of cold or heated air through geometrically modeled nozzles, small rocket motors, radial gas injection, and solid surfaces with simulated plume shape (either calculated or determined from Schlieren photographs of jet plumes). Shortcomings inherent in these methods can be traced to failure to account for all, or part, of such factors as plume deflections, mass entrainment, wake closure, influence of specific heat ratio, viscous effects, geometry, and temperature. It is, of course, not feasible to take account of all the contributing parameters simultaneously in a simulation test. While certain methods of plume simulation appear to be more appropriate than others, i.e., cold gas rather than solid surfaces, only limited comparisons have been undertaken between results for a simulation model and actual proto-

---

*) Numbers in brackets refer to entries in REFERENCES

type. In addition, documentation of the importance of individual factors such as plume geometry, plume stiffness or jet surface Mach number, and wake closure conditions for the various Mach number regimes has been lacking.

It is the purpose of this project to undertake, in close cooperation with the Gas Dynamics Laboratory at University of Illinois at Urbana-Champaign, the evaluation of modeling techniques [17] and importance of primary and secondary factors. To this end, it is essential that accurate and well controlled test results be available. Thus, the test conditions must be well known in terms of the wind tunnel working conditions and allow for careful control of the modeled propulsive jet, throat sonic condition, nozzle design methodology, local accelerations and Mach number distribution at the nozzle exit plane, and the working fluid.

The project was proposed [4] and is granted as a three year program. During the first year the design and construction was accomplished of a facility for the use of superheated Freon ($\gamma \approx 1.16$) at high pressure to be used for jet simulation in the FFA $0.5 \times 0.5 m^2$ S5 wind tunnel. Shake-down testing of the facility was started and an existing strut-supported axi-symmetric model was modified for tests with heated Freon. The activities during the first year have been reported [5, 6]. A second semi-annual status report [7], covering the scientific work accomplished during the period 1 Jan 1979 - 30 June 1979, has been issued for internal management use only. Most of the material presented in [7] is however included in this report, which covers the second year activities.

This report briefly describes the simulation test facility, the systems performance tests accomplished and the modifications made to the facility. The analytical basis for the plume modeling methodology proposed by Korst [8, 9] is reviewed. The results of tests at Mach number 2.0 and zero angle of attack with Freon of two nozzles designed in accordance with this method are presented and discussed.

2. SIMULATION TEST FACILITY

2.1 Introduction

A jet simulation test facility has been designed and constructed for use primarily with the FFA 0.25 m^2 S5 wind tunnel at supersonic free stream Mach numbers. It is possible to add an insulated and heated extension in the future for use with the FFA 1.0 m^2 S4 wind tunnel at transonic free stream Mach numbers. The unit has been constructed exclusively for this research project with the objective of allowing critical evaluation of the merits and limitations of plume modeling techniques. The facility is designed for various types of heated Freon but can in principle also be used in future investigations for other gases (i.e. Argon) with small changes in the instrumentation. Description of the facility with details of component design and construction are presented in the 1st Annual Report [6] along with a discussion of the temperature control requirements and system developed for this purpose.

2.2 Systems performance tests

Upon completion of the facility in December 1978 initial shakedown tests to check the mechanical functions of the facility were undertaken. During the period covered by this report a more extensive program to assess the performance of the facility has been carried out. To a large extent it has been possible to coordinate these tests with the start-up of the plume investigation program.

The performance of the facility is largely as expected. In particular, the simple convection type heater (Figure 1) has proved to be effective. Some minor modifications have, however, been necessary and these are briefly discussed below.

The insulation (8)*) of the heater (7) was severely less effective than specified. It was evident that extensive convection occurred within the insulation, thereby increasing the heat losses by a factor of at least five. This has the effect of prolonging the heating-up time, in particular when high temperatures are desired. The insulation was improved by additional packing of insulation material at two levels where easy access through the cover is possible. This remedy was fairly simple and reduced the convection efficiently.

A timer has been installed to start the heater prior to normal working hours. Due to the elaborate automatic temperature control system with its associated over-temperature activated power shut-off switches, this procedure is considered perfectly safe.

The Freon charging pump (14) has been furnished with a second pressure tap leading to the heated part of the facility. This modification is merely a matter of convenience for the operators of the rig - the heater may now be charged independent of the pressure within the cold part of the system.

Pressure activated switches have been installed in both the suction and pressure lines of the pump. The suction line switch closes down the pump below the set-point pressure, thereby protecting the pump from possible damage due to insufficient inlet pressure. The pressure line switch closes down the pump above the set-point to avoid unnecessary blowing of the safety valve.

Additional heating elements (17) have been installed on the model feed-line as close as possible to the model. This preheating is more effective than heating by letting a small air flow pass through the model as was first attempted.

---

*) Numbers in circles refer to item-list in Figure 1

The pressure-time history recorded in the model during a blow-down (Figure 2) shows at first a pressure drop and then a positive gradient during the larger part of the run. The pressure drop in the beginning of the run starts the flow of cold Freon from the unheated part of the system (4) into the heated part (7), where the high density cold Freon is being heated to a temperature close to that of the heated tubes. The lag in the heating process is so large that in the beginning of the run the mass flow of cold Freon into the heated section is appreciably larger than the mass flow of heated Freon into the model. When the delayed heating of the cold Freon becomes appreciable the pressure begins to rise. After a short time when the pressure in the heated part is equal to the pressure in the cold part, the inflow of cold Freon to the heated part stops and thereafter the flow is reversed, i.e. low density heated Freon flows from the heated to the cold part. The pressure loss caused by the low density flow is evidently so large that the total outflow is insufficient to compensate for the volume increase of the cold Freon that already has entered into the heated part, and consequently the pressure continues to rise. The force necessary to accelerate the cold Freon is also a contributing factor to the pressure rise.

It is possible to counteract the pressure increase by operating the main valve (11) during the run, as demonstrated in Figure 2. The solution to the problem has been, however, to use fast response transducers instead of the Scanivalve for measurement of those pressures, which are affected by the jet stagnation pressure. Combined with synchronized Schlieren photographs, the current procedure allows a range of pressure conditions to be monitored in a single run as the stagnation pressure varies.

In Figure 3 is shown a temperature-time history in the heated tube array (7) during a heating cycle. Air was used as the medium. It can be seen that convection takes place with a temperature

difference of just 15-25^{o}C between the directly and indirectly heated tubes. The relatively slow temperature increase is due to the substantial mass of the tubes being heated - the iron mass was near room-temperature when the heating was started. Immediately after a run considerable heat is left stored in the iron mass. The heating process is then mainly a matter of heating gas, a much faster procedure.

3. REVIEW OF THE PLUME MODELING METHODOLOGY SUGGESTED BY KORST

Integral and component approaches to near wake solutions, with their wake closure conditions linked to second law concepts, have led to a basic understanding of the problem and even to the establishment of relations [10] accounting for the influence of all pertinent variables. The difficulty of making specific assessments concerning the wake closure has led to extensive experimental studies in support of semi-empirical relations to account for the incomplete realignment of streamlines during recompression [11].

Experimental programs require proper plume simulation whenever the use of prototype propellant is not feasible. The modeling of plume interactions requires in principle geometrically congruent inviscid jet contours and correct pressure rise-jet boundary deflection characteristics (plume stiffness) as well as mass entrainment along the wake boundaries. Thus modeling with gaseous plumes is needed and normally involves dissimilar specific heat ratios.

The importance of generating the correct jet plume geometry has been stressed in prior efforts to establish modeling laws between propellant gases having dissimilar specific heat ratios [12, 13, 14]. However, the geometrical requirements were only formulated for the initial deflection angle of the jet, a condition not stringent enough to cope with plume induced separation [12].

The analysis of axisymmetric centered expansion [15] forms the basis for geometrical jet plume surface modeling [8]. This approach allows to match not only initial deflection angle but plume radius of curvature (shape), see Figure 4. It can be shown that the accuracy attained by such a procedure extends well beyond the range of convergence for the corner expansion itself [16].

The plume expansion derives its initial conditions from the flow approaching the end of the nozzle. For the case where exit conditions can be sufficiently well described, locally (M_L, θ_L), by conical source flow, sweeping simplifications in the interpretation of results are possible [16]. The solutions lead to a direct correspondence of nozzle plume shapes producing the same plume boundary geometry with one free parameter remaining available for satisfying the inviscid recompression conditions at the end of the separated flow region. It is thus possible to determine nozzle exit conditions in terms of Mach number at the nozzle lip and the nozzle divergence angle at the lip which will geometrically duplicate the jet contour produced by a gas with different specific heat ratios as it expands from a given nozzle under specific adjacent conditions (within the present degree of approximation), that is

$$\theta_{F,M} = \theta_{F,P} \quad \text{and} \quad R_{C,M} = R_{C,P} \tag{1}$$

where the geometry and notation are shown in Figure 5 and subscripts M and P are for model and prototype respectively. The downstream specifying condition should properly account for the viscid aspects of the base flow problem in their interaction with the inviscid components. With only one choice available as a result of the geometric requirements, it is obvious that one has to account above all, for the proper pressure rise in the external flow [12]. The recompression mechanism of the dissipative boundary of the jet, as a consequence of its mass entrainment characteristics, will, however, generally not be simultaneously

satisfied. While this effect may be expected to be small for cases involving strongly underexpanded plumes [16], it is possible to account for it in principle by introducing mass bleed. The concept of equivalent mass bleed has been shown [11] to be useful for both mass and temperature effect simulations.

The effect of plume stiffness has been examined in some detail [17] in tests carried out at FFA and at Calspan [18]. The results underscore the importance of the selection of plume flexibility characteristics to the simulation process particularly at supersonic Mach numbers. Selection of the pressure rise-deflection characteristics of the plume leads to the inviscid specifying relations [8].

$$[\gamma_M M_{F,M}^2 / (M_{F,M}^2 - 1)^{1/2}] = [\gamma_P M_{F,P}^2 / (M_{F,P}^2 - 1)^{1/2}] \qquad (2)$$

for weak shock recompression and

$$[2\gamma_M M_{F,M}^2 - (\gamma_M - 1)]/(\gamma_M + 1) =$$

$$[2\gamma_P M_{F,P}^2 - (\gamma_P - 1)]/(\gamma_P + 1) \qquad (3)$$

in case a strong shock occurs.

It is now necessary to identify the type of separation phenomenon to be investigated in order to establish design criteria for proper modeling. For a known pressure distribution over the prototype afterbody due to the non-separated slipstream, one can estimate the pressure rise due to separation by utilizing information on free interactions [11] or slight modifications thereof due to local pressure gradients and/or surface slope discontinuities. The resulting plateau pressure determines the jet surface Mach number $M_{F,P}$ so that the prototype conditions (nozzle flow, $M_{L,P}$ $\theta_{L,P}$ especially for conical source flow) are all given and the model jet surface Mach number $M_{F,M}$ (Eqs.(2) or (3)) are determined.

For this "design point", Eqs. (1), (2), or (3) are satisfied.

In the vicinity of this design point, only the more stringent condition of plume slope matching is retained. This can be expressed in the form of

$$\theta_{F,M} = \theta_{F,P} \tag{4}$$

and

$$\omega_{F,P} = \theta_{L,M} - \theta_{L,P} + \omega_{L,P} - \omega_{L,M} + \omega_{F,M} \tag{5}$$

Since the nozzle flows - and therefore $\theta_{L,M}$, $\theta_{L,P}$, $\omega_{L,M}$, $\omega_{L,P}$ - remain identical for design and off-design operation while one may expect that the wake pressure ratios shall still be closely modeled

$$p_b/P_E\Big|_P = (p_b/P_E)_M = f(PO_{I,M}/PO_E) \tag{6}$$

one finds the pressure ratio for the prototype flow from the Prandtl-Meyer relation

$$M_{F,P} = f(\gamma_P, \omega_{F,P}) \tag{7}$$

and the identity

$$P_{oI,P}/P_{oE} = (P_{oI,P}/p_b)_{M_{F,P}} \cdot (p_b/P_E)_M \cdot (P_E/P_{oE})_{M_E} \tag{8}$$

Thus, for each model flow experiment series for which the relations

$$(p_b/P_E)_M = f[M_E, (P_{oI,M}/P_{oE}), \gamma_M] \tag{9}$$

has been established, the corresponding operating condition of the prototype flow can be determined.

4. EXPERIMENTAL PROGRAM

4.1 Wind tunnel models

The compatibility of the Freon plume facility with the models reported on by the FFA in earlier jet interaction series of experiments provides a base of well defined prototype conditions to be modeled while furnishing the information necessary to critically evaluate the accuracy and applicability of the methodology discussed in Section 3.

The strut supported wind tunnel model for the study of slipstream plume interference effects used in the prototype air series [18] had to be modified to allow the high pressure heated Freon to be introduced to the model with minimum piping losses. The latter requirement is important since modeling from air as prototype, to Freon, as model, requires higher pressure ratios for the latter.

Figure 6 shows both the original configuration and modified versions of the model and Figure 7 is a photograph showing the modified model mounted in the wind tunnel and Figure 8 depicts the location of pressure taps on the boat tail.

The model body, boattail, and base region - the basic configuration being an 8^{0}-degree boattail with L/D = 1 [18,19] - are instrumented with pressure taps. As mentioned in Section 2 the individual pressures, which are affected by the jet stagnation pressures, are recorded from a series of fast response transducers, while the rest of the pressures are recorded from a Scanivalve. Combined with Schlieren photographs (and in some cases oil flow photographs), this allows the accurate determination of the external flow-jet interference pattern. In particular, location of the plume induced separation on the afterbody is a very sensitive measure of plume interference effects and of the accuracy obtained by use of the proposed modeling methodology.

Based on earlier series of experiments conducted with air nozzles [18,19,20], calculations were carried out according to the methodology of Section 3 to select the most suited prototype configuration for initial Freon 22 modeling tests with both weak and strong shock closure conditions. The results mapped into the Freon facility performance plane are shown in Figure 9. Based on these calculations, the air nozzle with a nominal exit Mach number of 2.5 and a conical wall angle of 10° was selected as the first prototype (see Figure 10a). Design conditions were chosen to allow for both design and off-design experimentation with the Freon nozzles for weak ($M_{L,M} = 3.9$, $\theta_{L,M} = 19.76^{\circ}$, $P_{oI}\big|_M = 12.83$ MPa, see Figure 11a, corresponding to $P_L/P_E\big|_A = 6.1$) and strong ($M_{L,M} = 3.19$, $\theta_{L,M} = 14.19^{\circ}$, $P_{oI}\big|_M = 5.69$ MPa, see Figure 11b, corresponding to $P_L/P_E\big|_A = 9.20$) shock closure condition. Operating ranges for these model tests are shown in Figure 9.

Computer calculations using the method of characteristics following transonic flow solutions for the nozzle throat region have been carried out, confirming the validity of conical source flow approximations near the lip for both prototype and model nozzles [7, 16].

4.2 Calibration tests

While the earlier strut configuration produced only negligible interference effects, as has been confirmed by comparison with sting mounted runs, it was anticipated that the new additional Freon piping and its enlarged fairing might cause noticeable interference effects. This was checked in tests with air as propellant using two nozzles for $M_L = 2.5$; $\theta_L = 10^{\circ}$ and 20° as shown in Figure 10. The pressure distribution on an 8° conical boat-tail of length one diameter was measured and Schlieren photographs were taken with variation of the lip pressure ratio P_L/P_E.

The measured pressure distributions for the two nozzles are shown for a lip pressure ratio with separated flow on the boat-tail in Figure 12 in comparison with the earlier test results. The difference between the two tests, which is probably mainly due to the different interference from the support strut, is small but measurable. The Schlieren photographs reveal that the extension of the separated region seems to be nearly unaffected. The base pressure is for $\theta_L = 10^o$ changed from $P_b/P_E = 1.35$ in the earlier test to $P_b/P_E = 1.30$ in the current test.

The small differences noted for the prototype air nozzle due to the modified strut required that the air prototype tests be repeated over the range reported in earlier papers to guarantee that strut effects did not introduce unanticipated changes. The results from the current air tests are shown in Figure 13. The results from the earlier tests are also shown for comparison.

The base pressure from the earlier air tests were used when calculating the shapes of the Freon nozzles manufactured for the modeling tests. Recalculations using the base pressure from the current air tests have revealed, that the change in the modeled nozzle lip angle is too small (approximately 0.60 degrees) to justify construction of new nozzles for the current tests.

4.3 Plume modeling experiments

Tests were carried out with the two Freon nozzles for weak and strong shock closure conditions respectively with Freon 22 as propulsive gas at a free stream Mach number of 2.0 and at zero angle of attack. The stagnation pressure $P_{oI}\big|_M$ was varied in a wide range around the design pressure ratio and the stagnation temperature was kept in the range 200-250^{o}C. The free stream stagnation pressure was atmospheric, the free stream stagnation temperature around 20^{o}C and the Reynolds number based on model

length of 6×10^6. The jet stagnation pressure and temperature were measured in the nozzle settling chamber.

A complete set of the model pressures recorded are presented in tables 1 - 6 in the Appendix. Typical pressure distributions for prototype and model nozzles at pressures close to the design conditions are shown in Figures 14 and 15. The agreement achieved between air prototype and the Freon model pressure distributions is good. The corresponding Schlieren photos, Figures 16 and 17 are seen to be nearly identical. A direct comparison of the essential features of the two flow fields from photo overlays are given in Figures 16c and 17c and the agreement is also satisfactory for shock and plume geometries along the entire near-wake region.

Shown in Figures 18 and 19 is the base pressure ratio P_b/P_E as a function of the jet stagnation pressure P_{oI} measured in the settling chamber of the nozzle. For the weak shock nozzle, the plume surface Mach numbers are sufficiently large at the higher stagnation pressures that, combined with the temperature loss in the model and its support, condensation has been found to occur in some tests and those points are flagged in Figures 18 and 22.

For comparison between the prototype air and the model Freon base pressures the relation P_b/P_E is plotted in Figure 20 as function of the lip pressure ratio P_L/P_E, which was computed. It is also possible to make the comparison in the Freon plane in the way, demonstrated in Figure 21 where Figure 21a shows the experimental results for the model nozzle, Figure 11a (weak shock modeling). The theoretical prototype curve is found with the help of Eqs. (4) through (9) which yield the corresponding stagnation pressures in accordance with Figure 21b.

Air prototype results transformed into the Freon model plane are for comparison plotted in Figures 22 and 23 together with

the replotted Freon model results (from Figures 18 and 19) and the design point is identified. From these results, it can be seen that the present modeling technique allows to conduct investigations of the plume induced separation phenomena with air at much lower nozzle-to-ambient stagnation pressure ratios than would be required for many conventional propellants as $\gamma_M > \gamma_P$ (note that in the present experimental program, the roles of model and prototype have been exchanged). It is also evident that with air as model gas, replacing the Freon in the present high pressure gas facility,very high prototype pressure ratios can be simulated.

Also shown are a few results for the Freon nozzles run with hot air to illustrate the shortcomings of retaining nozzle congruence. Slope modeling of these results gives reasonable correspondence to the prototype data but at effectively much lower pressure ratios. At this conditions, no separation essentially, the radius of curvature is less important. In contrast to the proposed technique based on distorted nozzle geometries, very high stagnation pressures would be required for modeling with gases of higher than prototype specific heat ratios. This in turn would restrict experimentation to lower-than-ambient base pressures in accordance with the limitations anticipated and stated in Reference [12].

The separation location S/D for the air prototype and Freon model nozzles are shown as a function of lip pressure in Figure 24 and with the air prototype results transformed into the Freon model plane in Figure 25.

While the modeled nozzles have been calculated for a single design condition, comparisons are made over the operating range of the tests to indicate off-design applicability of the modeling procedure. The strong shock nozzles appear to provide better correlation over a wider range for base pressure, Figures 20 and 23, than does the weak shock nozzle, Figures 20 and 22. For the more sensitive separation location, however, as shown in Figures

24 and 25, the weak shock nozzle provides the best correlation, particularly near the design pressure ratio. From Figure 24 it might possibly be concluded that the agreement between prototype and model results decreases with increasing lip pressure for both strong and weak shock closure conditions.

5. CONCLUSIONS

The high pressure, hot gas Freon jet simulation facility developed at the FFA is fully operational. It can be utilized for well controlled jet slipstream interference studies with a variety of gases simulating propellants. In particular, it allows to evaluate the merits and the potential of a plume modeling methodology suggested by Korst [8,16]. Equally important will be the ability to critically examine the wake closure conditions for the modeling procedure, including the possible requirements for equivalent mass bleed to account in greater detail for transport phenomena across the plume boundary.

The initial tests show good agreement with anticipated facility performance. The Freon plumes shapes have been found to be in close agreement with those of the corresponding air test supporting the suggested modeling methodology and design procedures.

While agreement between prototype and model experiments for base pressures was satisfactory not only for the design point but also for a rather wide range of off-design conditions, the more sensitive separation distance was equally well correlated, however, only for a narrower range, in the vicinity of the design point for the weak shock closure condition. Since the weak shock is physically realistic for the flow near the confluence point, this modeling scheme appears presently to be the most appropriate. The continuing experimental program will extend and allow further

critical evaluation of the modeling technique to a wide range of freestream Mach numbers.

Since the dynamic recompression modeling relations are not restricting to axisymmetric stream confluence geometries and as base pressures are practically constant in case of large separation regions, the simulation methodology should remain valid for afterbodies having more complex geometries and for cases involving appreciable angles of attack, $\alpha \neq 0$.

REFERENCES

1. Addy, A.L.; Korst, H.H.; Walker, B.J.; White, R.A. A Study of Flow Separation in the Base Region and Its Effects During Powered Flight. AGARD Conf. Proc. No. 124 on Aerodynamic Drag, AGARD-CP-124, Specialists' Meeting held at Izmir, Turkey, 10-13 April 1973.

2. Alpinieri, L.J.; Adams, R.M. Flow Separation due to Jet Pluming. AIAA J., Oct. 1966 (4), pp. 1865-6.

3. Deep, R.A.; Henderson, J.H.; Brazzel, C.E. Thrust Effects on Missile Aerodynamics. U.S. Army Missile Command Report No. RD-TR-71-9, May 1971, Redstone Arsenal, Ala., USA.

4. Nyberg, S.-E. Investigation of Modeling Concepts for Plume-Afterbody Flow Interactions. Research Proposal FFAA-77-4 to U S Army European Research Office, June 1977.

5. Nyberg, S.-E. Investigation of Modeling Concepts for Plume-Afterbody Flow Interactions. Grant DAERO-78-G-028, 1st Semi-Annual Status Report, 1 Jan 1978 - 30 June 1978. Internal report for ERO and FFA.

6. Nyberg, S.-E.; Agrell, J.; Hevreng, T. Investigation of Modeling Concepts for Plume-Afterbody Flow Interactions. Grant DAERO-78-G-028, 1st Annual Technical Report, February 1979.

7. Nyberg, S.-E. Investigation of Modeling Concepts for Plume-Afterbody Flow Interactions. Grant DAERO-78-G-028, 2nd Semi-Annual

7.	Nyberg, S.-E. (continued)	Status Report, 1 Jan 1979 - 30 June 1979. Internal report for ERO and FFA.
8.	Korst, H.H.	Approximate Determination of Jet Contours Near the Exit of Axially Symmetrical Nozzles as a Basis for Plume Modeling. TR-RD-72-14, August 1972, US Army Missile Command, Redstone Arsenal, Ala., USA.
9.	Korst, H.H.	An Analysis of Jet Plume Modeling by Dissimilar Propellant Gases. Proc., 43rd Semi-Annual Meeting, Supersonic Tunnel Association, 2-3 April 1975, Pasadena, Cal., USA.
10.	Korst, H.H. Chow, W.L. Zumwalt, G.W.	Research on Transonic and Supersonic Flow of a Real Fluid at Abrupt Increases in Cross Section (with Special Consideration of Base Drag Problems. Final Report. Report No. ME-TN-392-5. University of Ill., Urbana, Ill., USA, Dec. 1959.
11.	Carrière, P. Siriex, M. Delery, J.	Methodes de Calcul des Écoulements Turbulents Decolles en Supersonique. Prog. in Aerospace Sci., 1975, Vol. 16, No. 4, pp. 385-429.
12.	Goethert, B.H. Barnes, L.T.	Some Studies of the Flow Pattern at the Base of Missiles with Rocket Exhaust Jets. Arnold Engr. Development Center, Tullahoma, Tenn., AEDC-TR-58-12, June 1960.
13	Herron, R.D.	Investigation of Jet Boundary Simulation Parameters for Underexpanded Jets in a Quiescent Atmosphere. AEDC-TR-65-6, Arnold Engr. Development Center, Tullahoma, Tenn., Sept. 1968.
14.	Sims, J.L. Blackwell, K.L.	Base Pressure Correlation Parameters, presented at the workshop on Missile and Plume Interaction Flow Fields, Redstone Arsenal, Ala., 7-8 June 1977.
15.	Johannesen, N.H. Meyer, R.E.	Axially-Symmetrical Supersonic Flow Near the Centre of an Expansion. The Aero. Quarterly (2), 1950, pp. 127-42.
16.	Korst, H.H. Deep, R.A.	Modeling of Plume Induced Interference Problems in Missile Aerodynamics. AIAA Paper No. 79036, 17th Aerospace Sciences Meeting, New Orleans, La., 15-17 Jan. 1979.

17. Korst, H.H.
White, R.A.
Nyberg, S.-E.
Agrell, J.
The Simulation and Modeling of Jet Plumes in Wind Tunnel Facilities.
Paper to be presented at the AIAA 11th Aerodynamic Testing Conference, 18-20 March 1980.

18. Reid, C.F.
Effects of Jet-Plume and Pressure Distributions over a Cylindrical Afterbody at Transonic Speeds.
Calspan Report No. AA-5017-W-15, W.A. T17-160, T17-170, Feb. 1979.

19. Agrell, J.
White, R.A.
An Experimental Investigation of Supersonic Axisymmetric Flow over Boattails with a Centered Propulsive Jet.
The Aeronautical Research Institute of Sweden, FFA, Technical Note AU-913, Dec. 1974.

20. White, R.A.
The Calculation of Supersonic Axisymmetric Afterbody Flow with Jet Interference and Possible Flow Separation.
The Aeronautical Research Institute of Sweden, FFA, Technical Note AU-912, 1974.

21. White, R.
Agrell, J.
Boattail and Base Pressure Prediction including Flow Separation for Afterbodies with a Centered Propulsive Jet and Supersonic External Flow at Small Angles of Attack.
AIAA/SAE 13th Propulsion Conference, Orlando, Florida, 11-13 July 1977.

ACKNOWLEDGEMENT

The authors wish to thank Professor H.H. Korst and Professor R.A. White at the University of Illinois for stimulating and fruitful cooperation and for their contributions to this report.

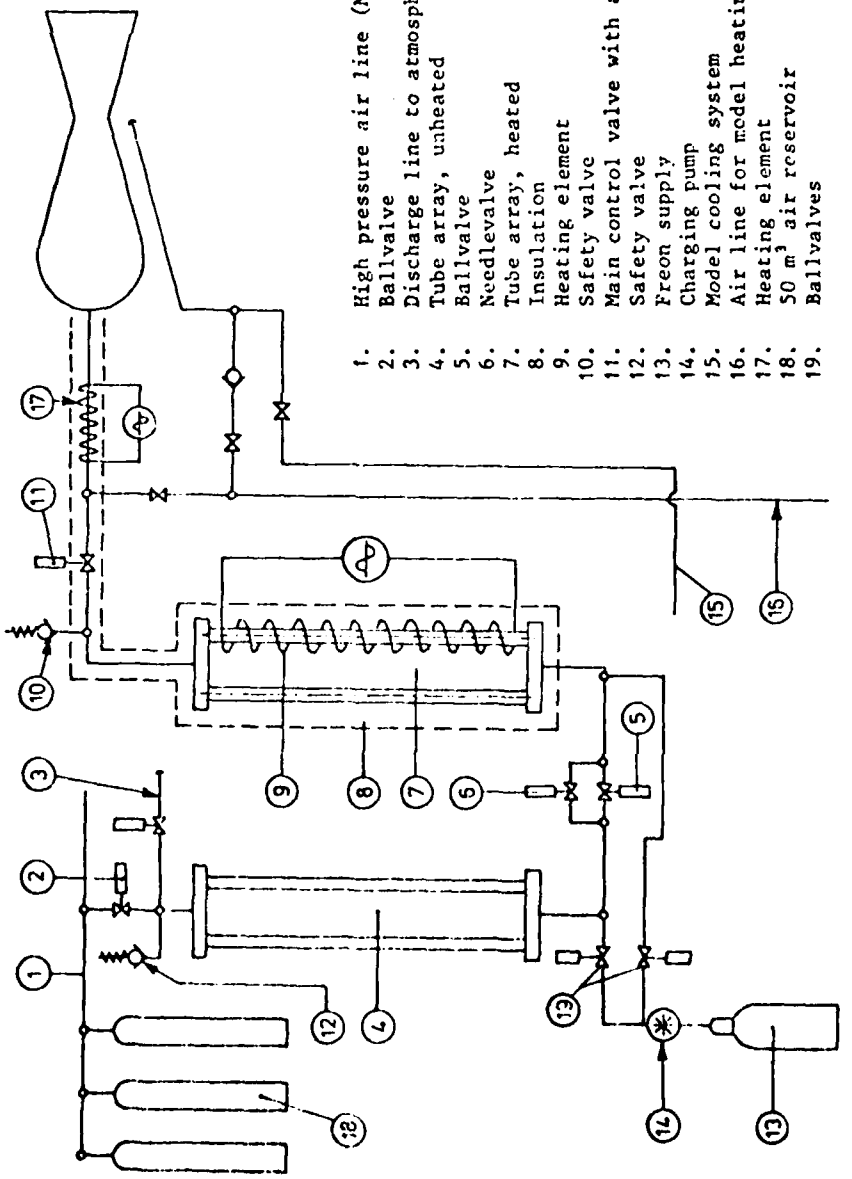

Figure 1. Annotated schematic of air driver system, Freon heater and nozzle.

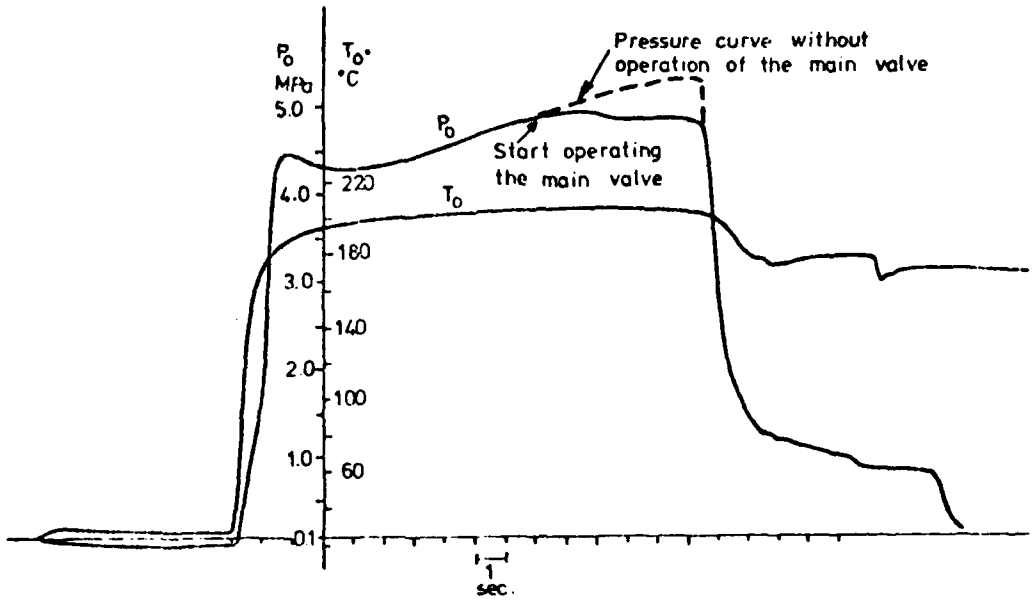

Figure 2. Jet stagnation pressure P_o and temperature T_o during a run.

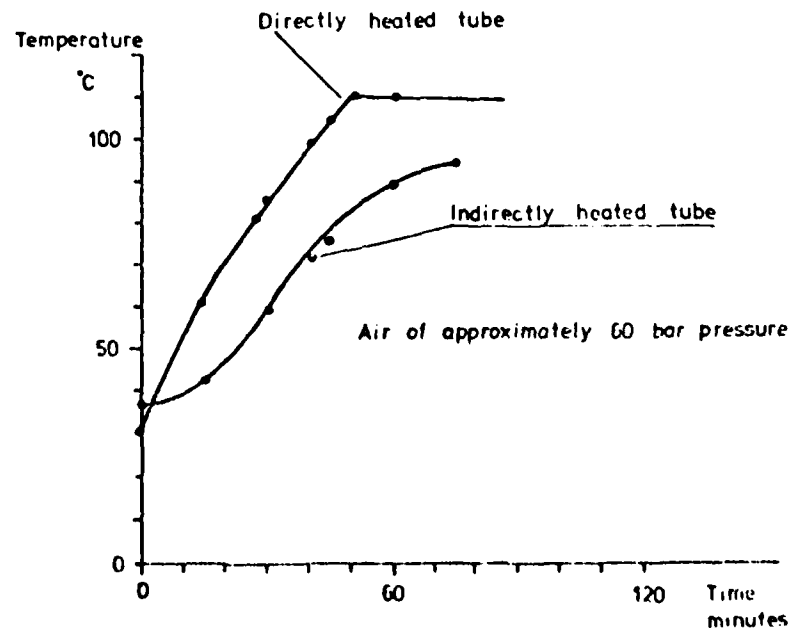

Figure 3. Wall temperatures in the heated tub array during a heating cycle.

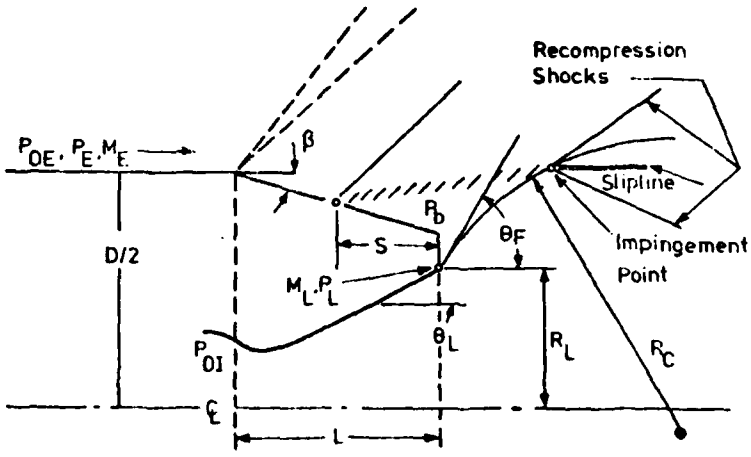

Figure 4. Flow configuration for plume induced separation from conical afterbody (Geometrical and Operational Parameters Identified).

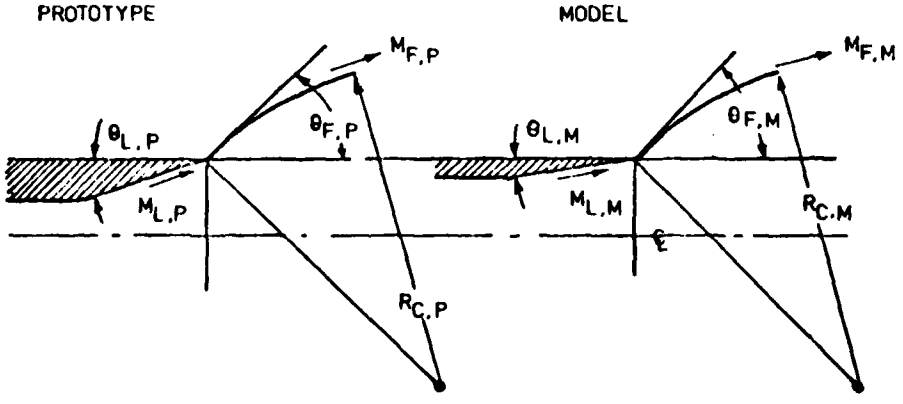

Figure 5. Schematic of geometrical plume modeling [16].

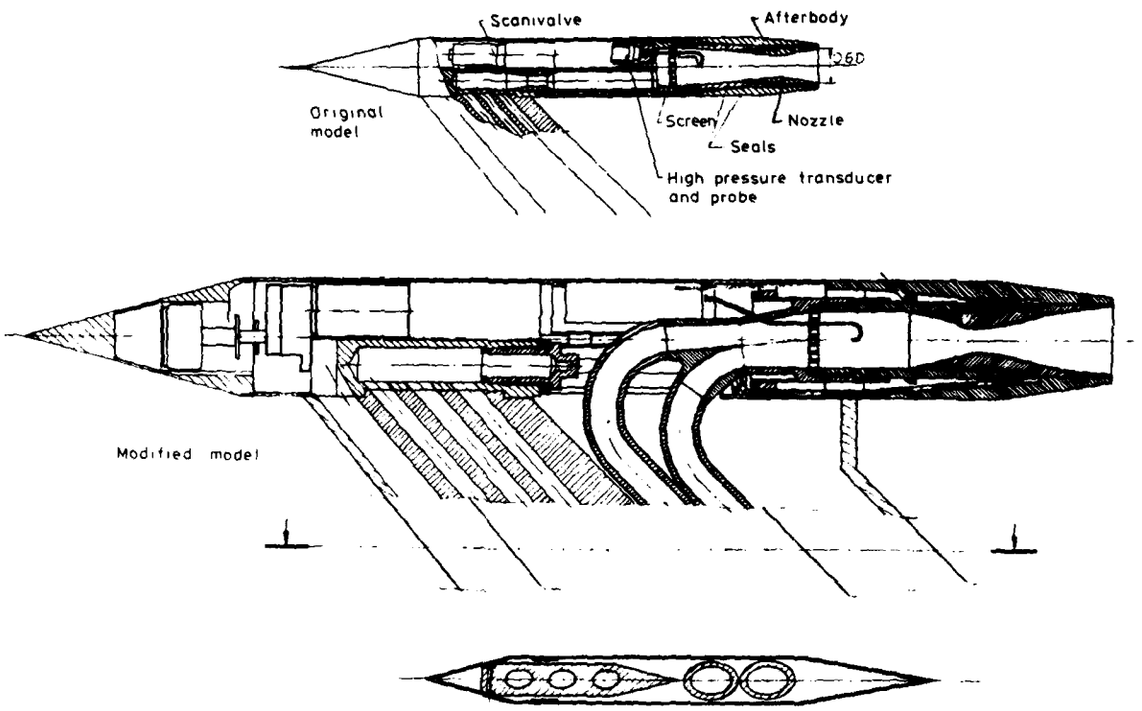

Figure 6. Adaption of propulsive afterbody wind tunnel model for operation with Freon.

Figure 7. Model installation with leading and trailing edge fairings of the support strut in position but with side plates removed.

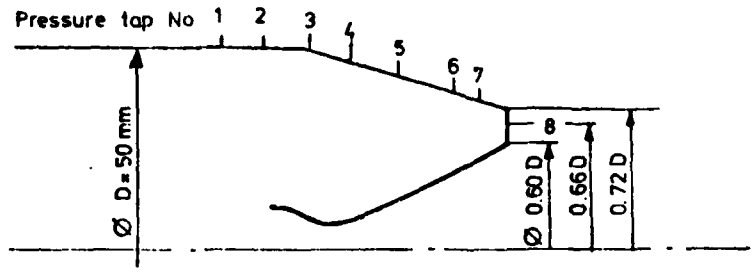

Pressure tap No	X/D
1	8.10
2	8.30
3	8.52
4	8.74
5	8.96
6	9.20
7	9.42
8	9.50

Figure 8. Location of pressure taps on boat-tail.

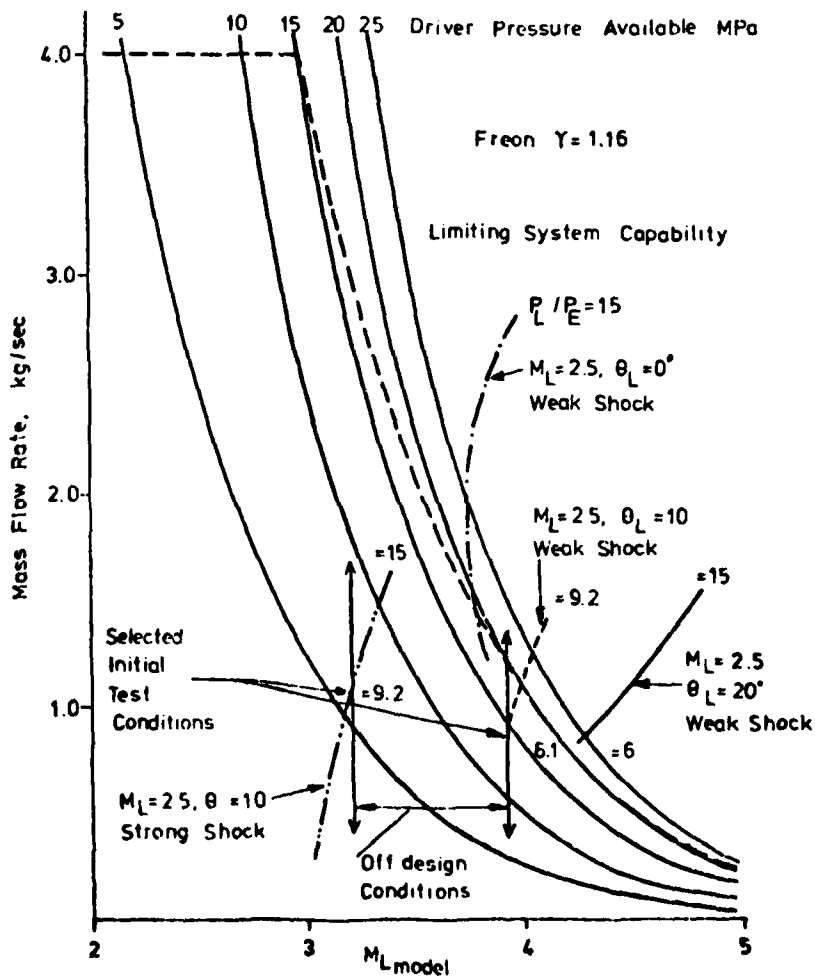

Figure 9. Modeled performance and test configurations for initial test program.

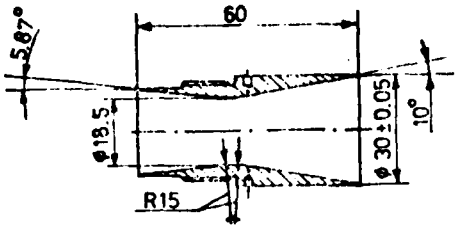

a) $M_L = 2.5$, $\theta_L = 10°$

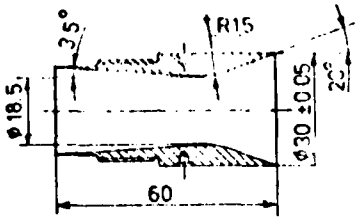

b) $M_L = 2.5$, $\theta_L = 20°$

Figure 10. Nozzles for calibration tests.

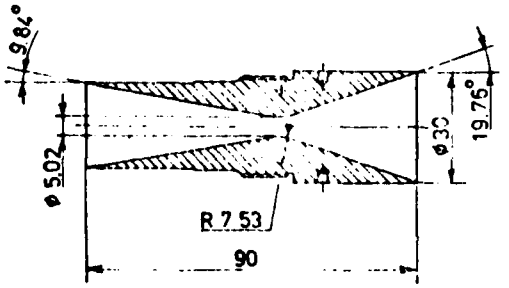

a) Weak shock modeling $M_L = 3.90$, $\theta_L = 19.76°$

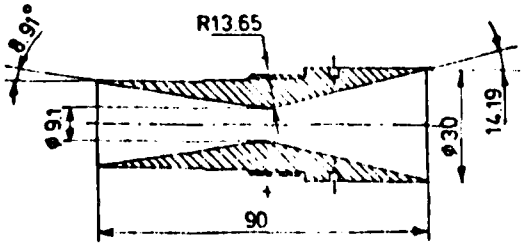

b) Strong shock modeling $M_L = 3.19$, $\theta_L = 14.19°$

Figure 11. Nozzles for modeling tests.

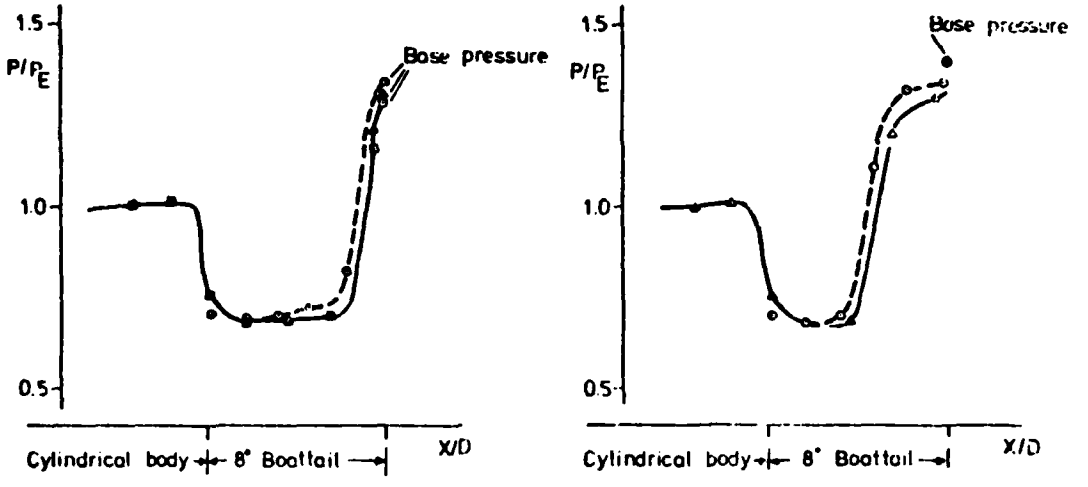

○ 31784 Air M_L=2.5 θ_L=10° P_L/P_E=9.2 earlier test
▲ 35260 Air M_L=2.5 θ_L=10° P_L/P_E=9.2 current test
□ 35312 Freon M_L=3.19 θ_L=14°19 P_o~4.8 MPa

○ 31751 Air M_L=2.5 θ_L=20° P_L/P_E=9.1 earlier test
△ 35268 Air M_L=2.5 θ_L=20° P_L/P_E=9.2 current test

Figure 12. Pressure distribution on the rear part of the body M_E = 2.0; α = 0; Effect of redesigned strut (Five Digit Numbers Identify Runs).

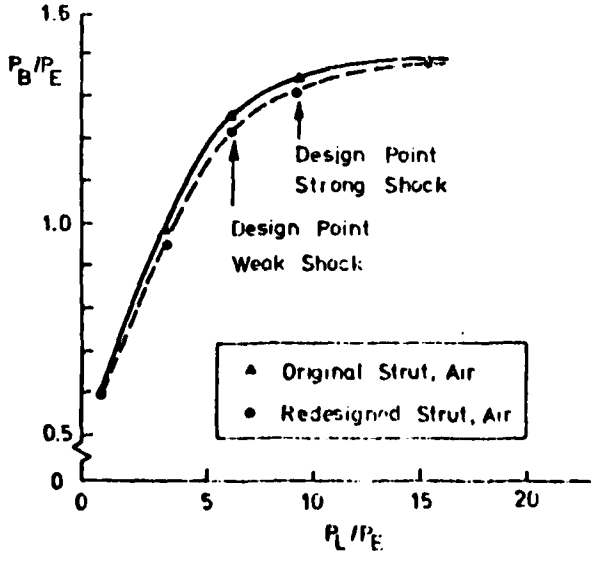

Figure 13. Base pressure ratio versus P_L/P_E for the air prototype nozzle ($\theta_L = 10^0$) showing effect of strut modification.

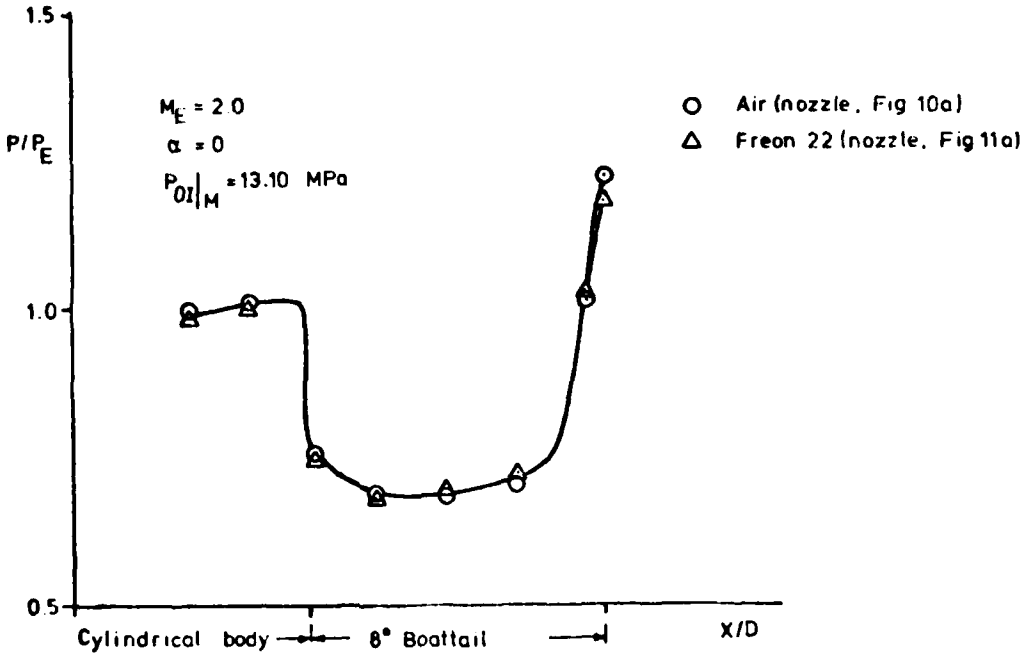

Figure 14. Pressure distribution on the rear part of the body at design condition (Weak Shock Modeling).

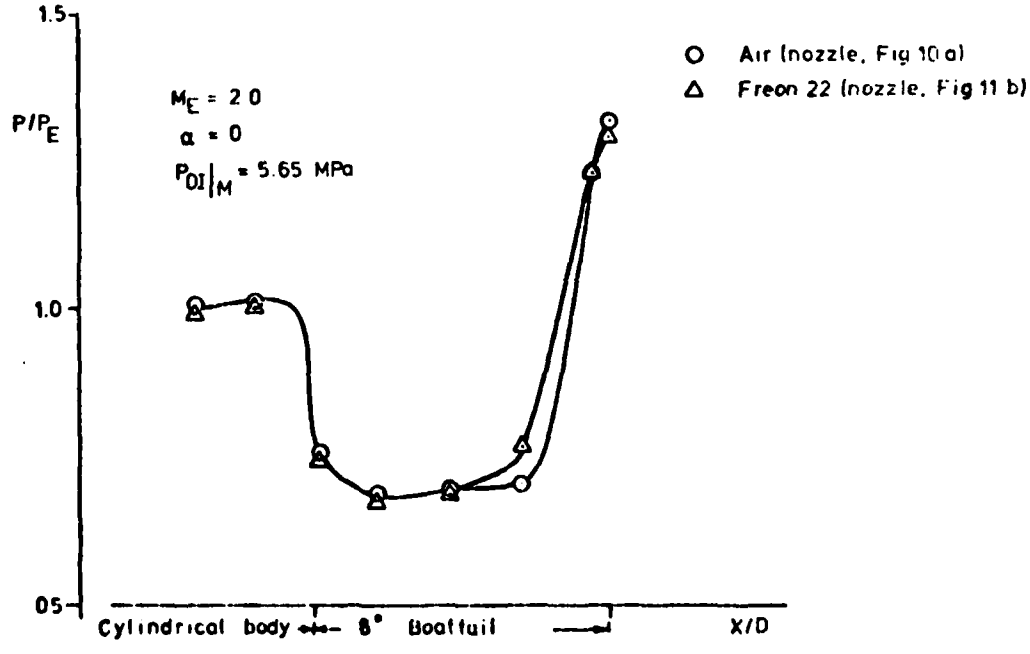

Figure 15. Pressure distribution on the rear part of the body at design condition (Strong Shock Modeling).

a) Run 35261 Air $M_L = 2.5$; $\theta_L = 10$; $P_L/P_E = 6.0$.

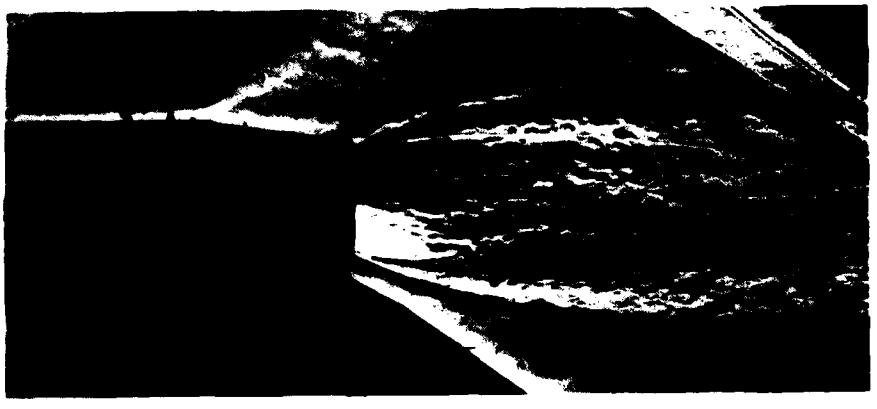

b) Run 35352 Freon 22 $M_L = 3.90$; $\theta_L = 19.76$; $P_{OI} = 13.10$ MPa.

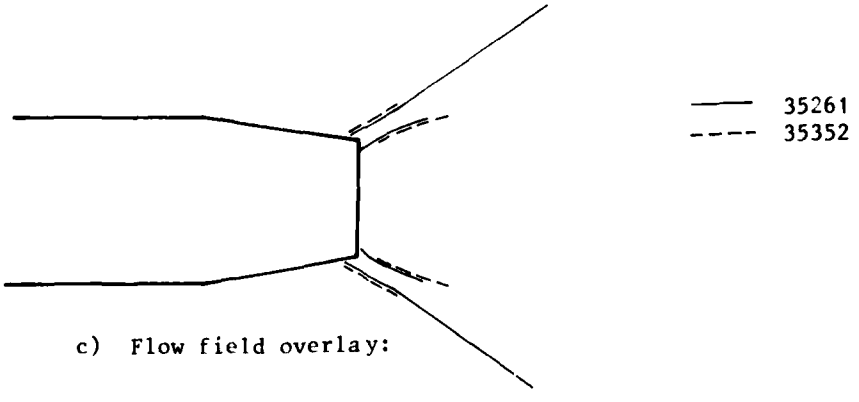

c) Flow field overlay:

Figure 16. Comparison of plume shape from Schlieren photos. $M_E = 2.0$; $\alpha = 0$. (Weak Shock Modeling)

a) Run 35260 Air $M_L = 2.5$; $\theta = 10$; $P_L/P_E = 9.2$

b) Run 35340 Freon 22 $M_L = 3.19$; $\theta_L = 14.19$; $P_{OI} = 5.65$ MPa

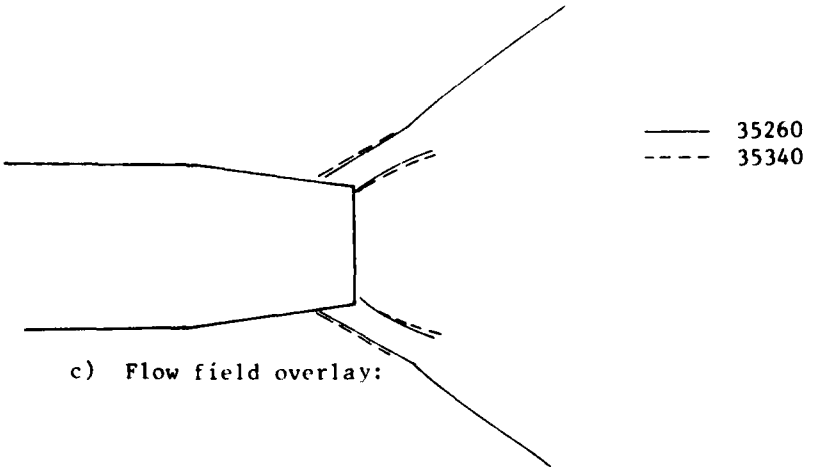

c) Flow field overlay:

Figure 17. Comparison of plume shape from Schlieren photos. $M_E = 2.0$; $\alpha = 0$. (Strong Shock Modeling)

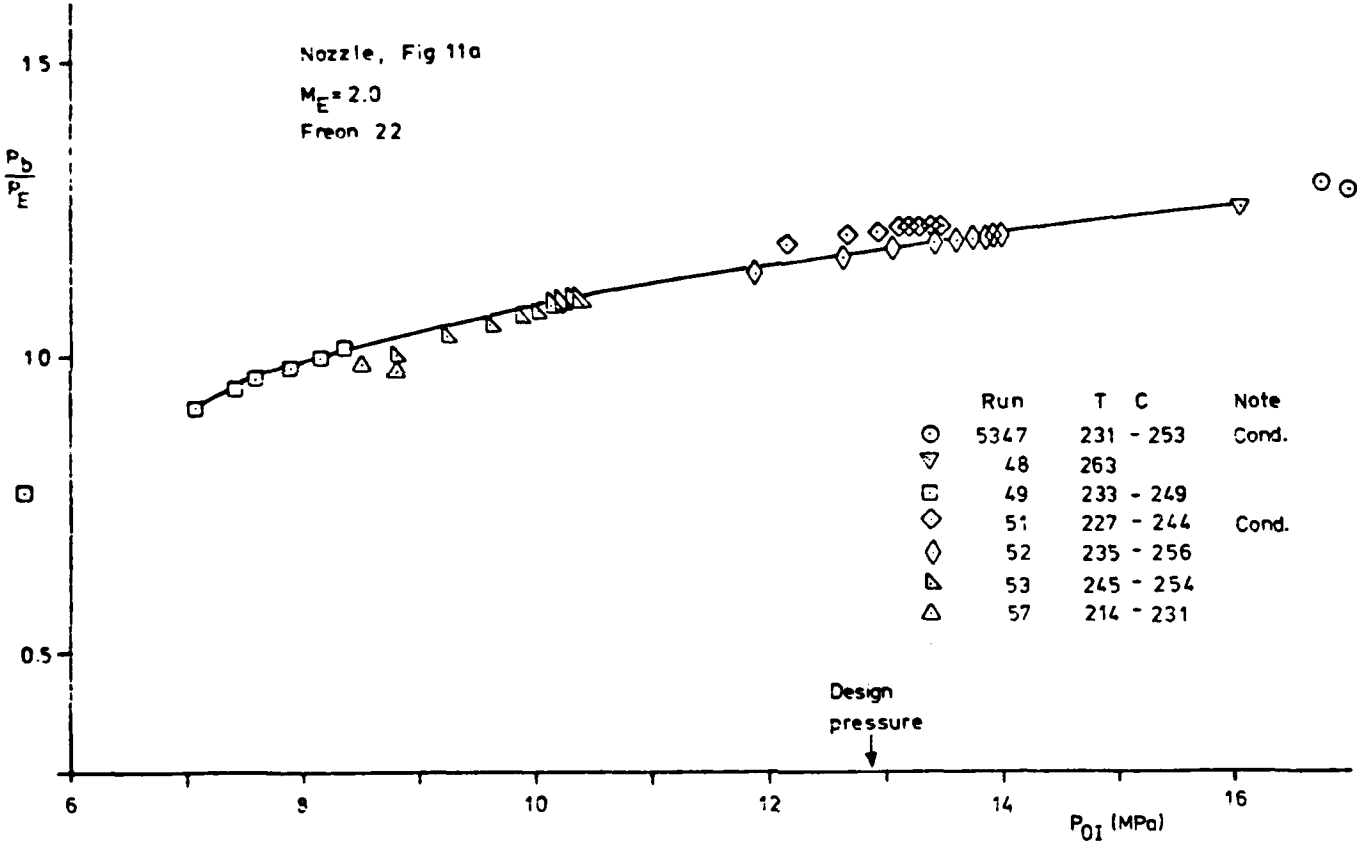

Figure 18. Base pressure P_b/P_E versus jet stagnation pressure P_{oI} for Freon nozzle (Weak Shock Modeling, Fig. 11a)

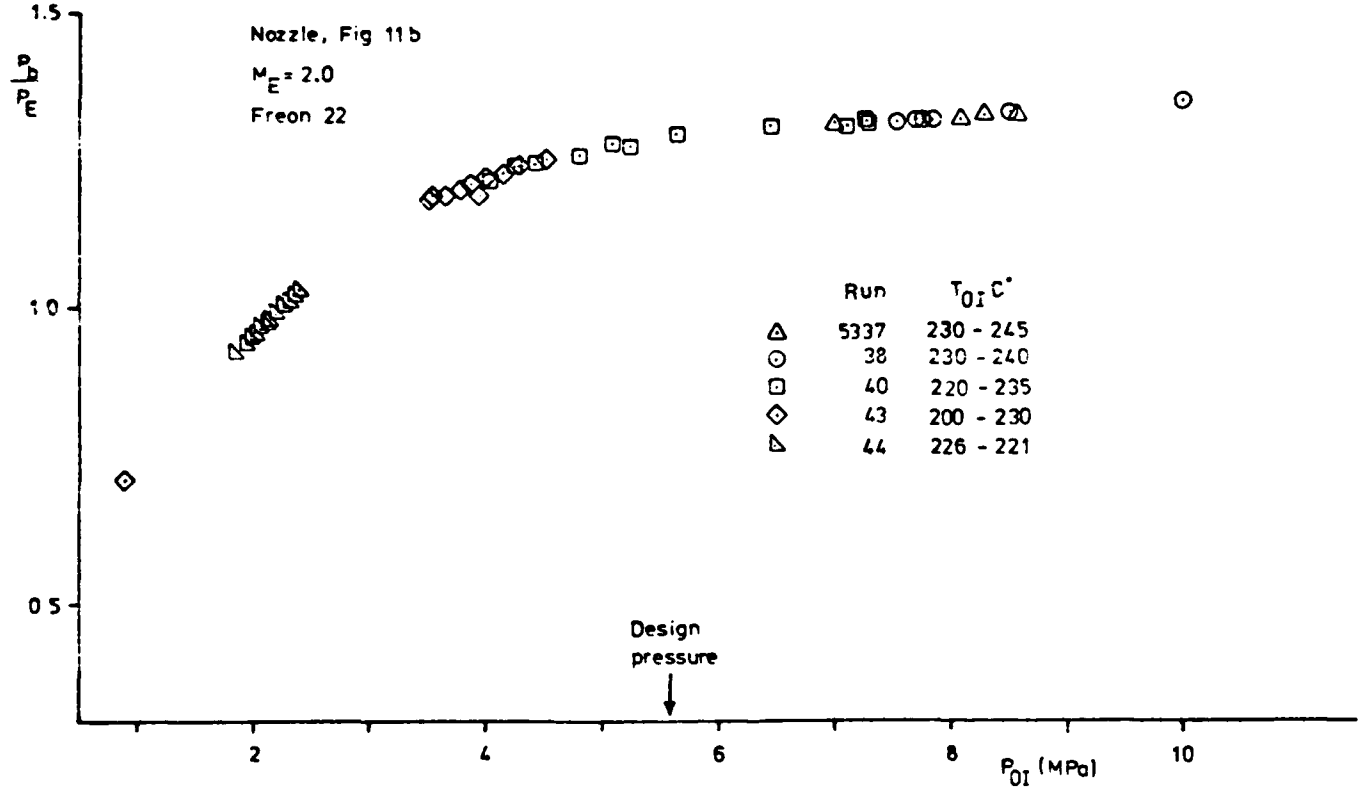

Figure 19. Base pressure P_b/P_E versus jet stagnation pressure P_{oI} for Freon nozzle (Strong Shock Modeling, Fig. 11b)

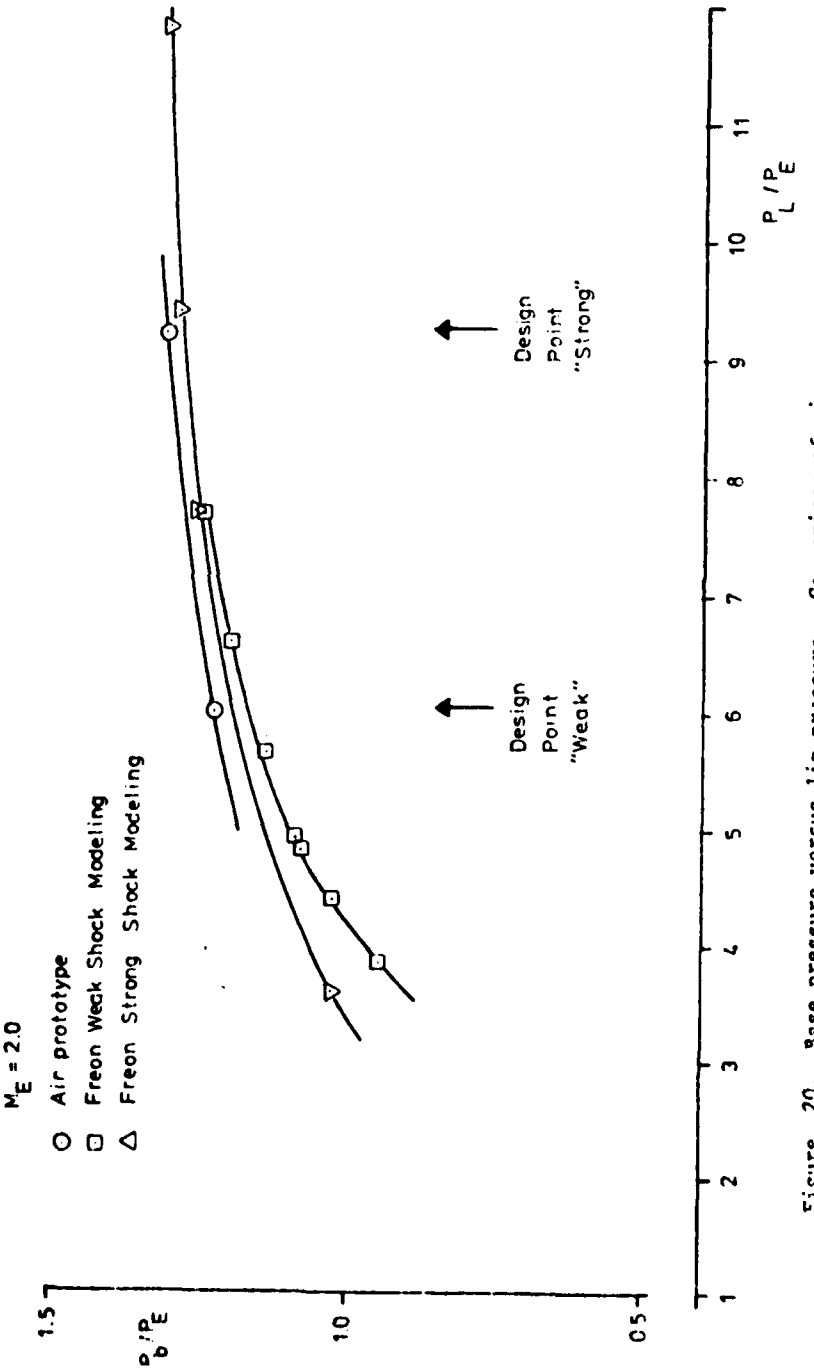

Figure 20. Base pressure versus lip pressure. Comparison of air prototype with Freon models.

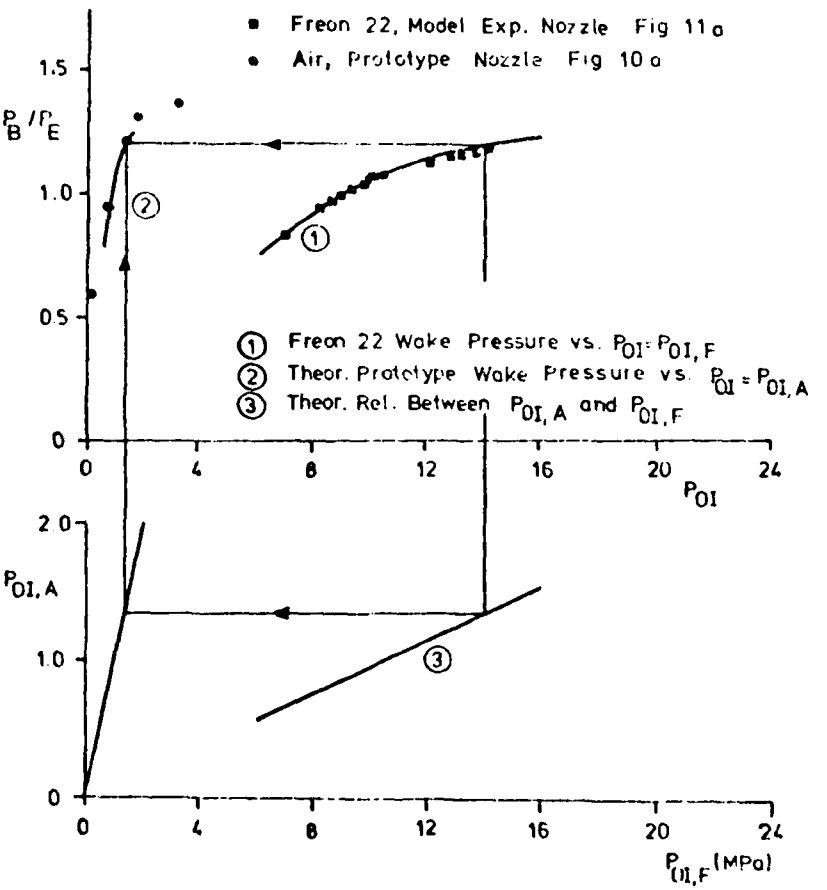

Figure 21. Correlation between prototype (Air) and model (Freon-22) test data (Weak Shock Modeling)

(a) Wake pressure ratio versus P_{oI}

(b) $P_{oI,A}$ versus $P_{oI,F}$ (Eqs. (1), (2), (4-9)

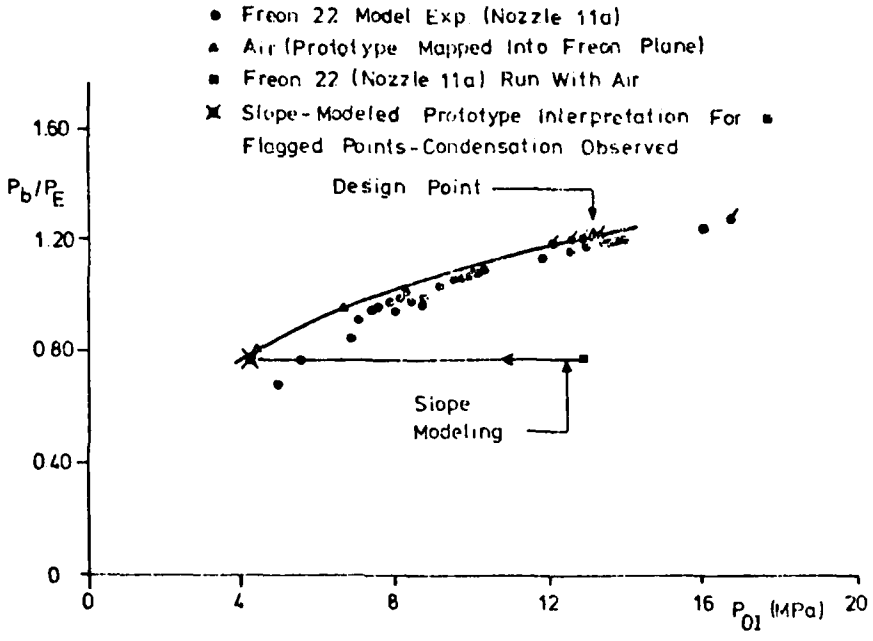

Figure 22. Wake pressure ratio versus Freon nozzle stagnation pressure (MPa) (Weak Shock Modeling)

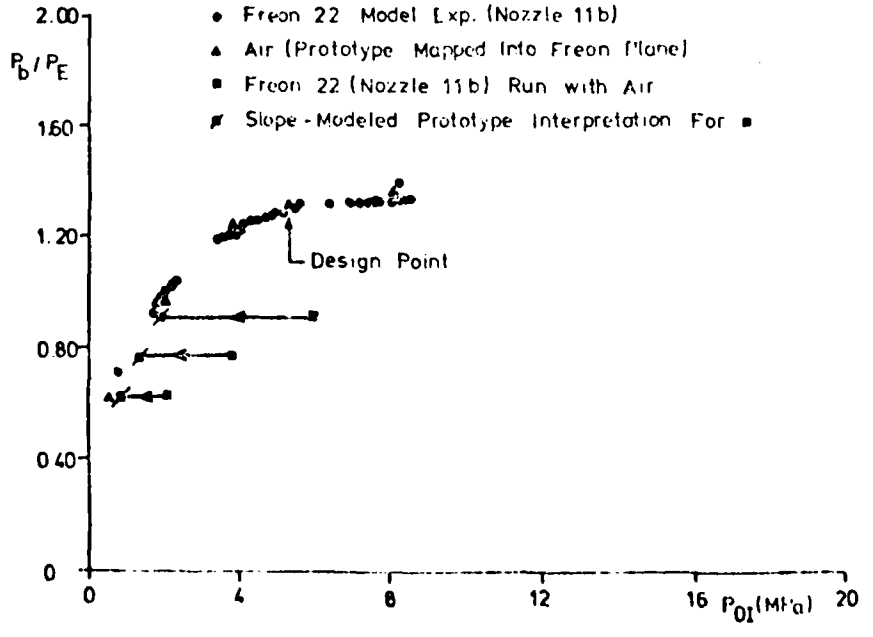

Figure 23. Wake pressure ratio versus Freon nozzle stagnation pressure (MPa) Freon-22 experiments (Strong Shock Modeling)

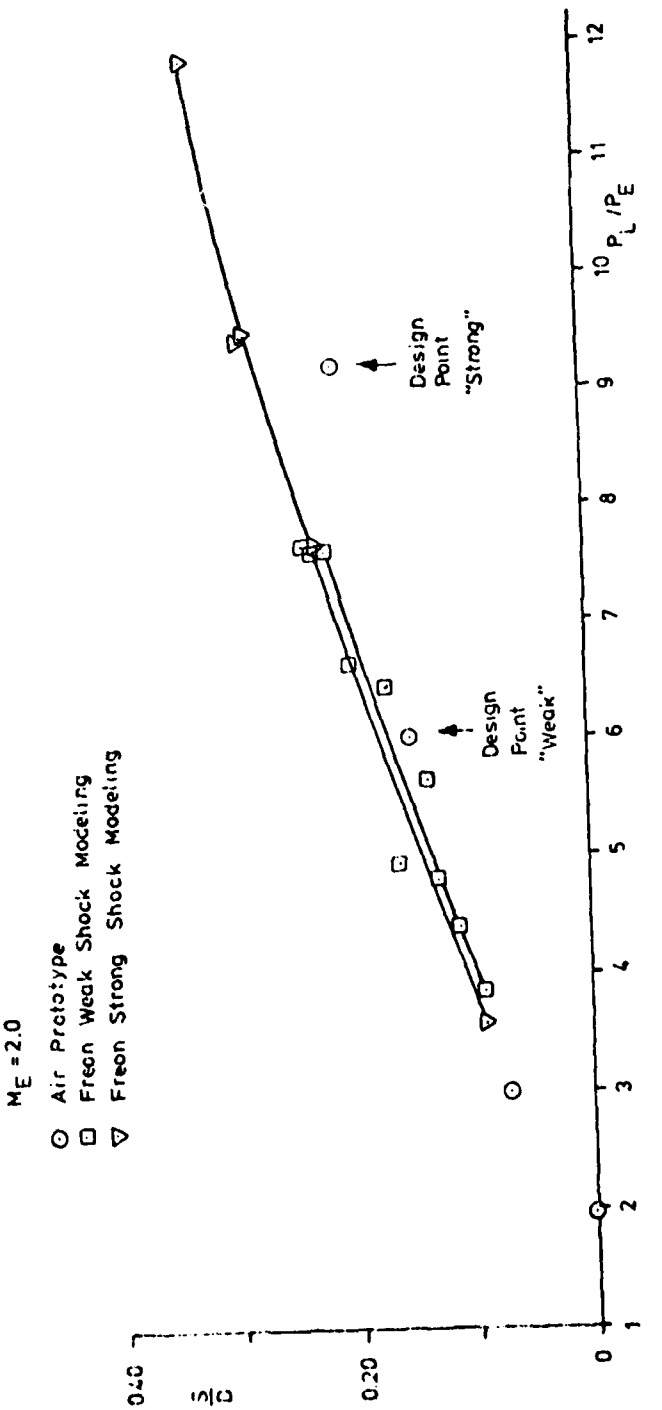

Figure 24. Separation location vs lip pressure for air prototype and Freon model nozzles.

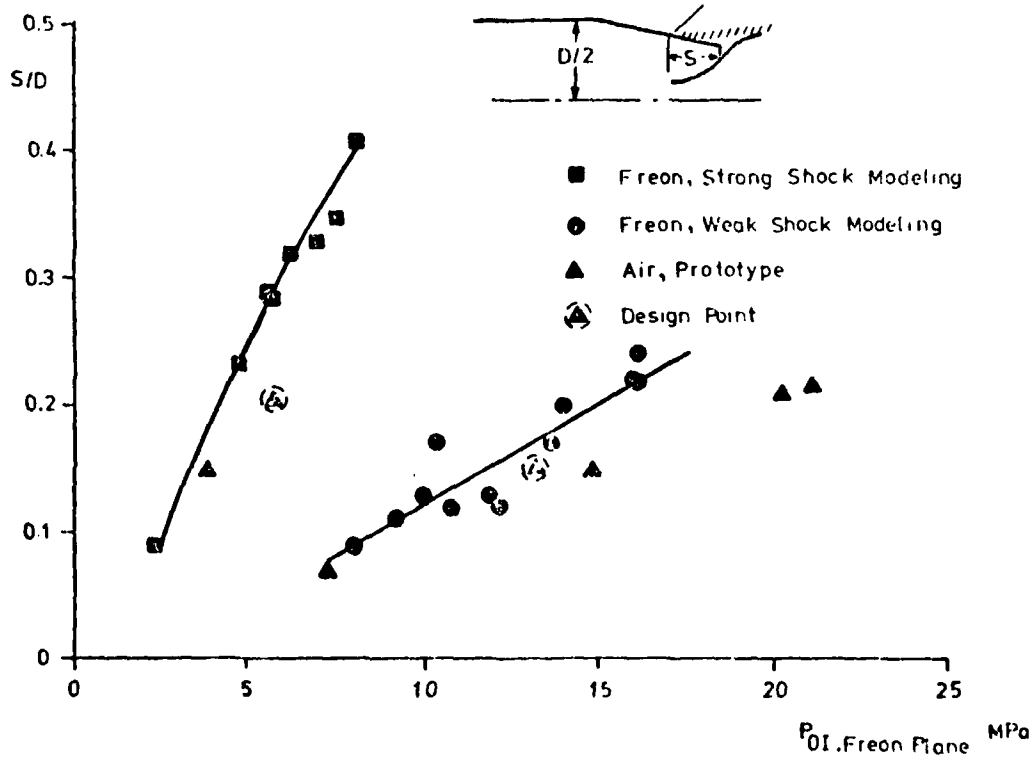

Figure 25. Separation distance vs. Freon nozzle stagnation pressure for air prototype and Freon-22, both strong and weak shock modeling, design and off-design.

APPENDIX

Table	M_L	θ_L	Test Gas
1	2.5	10	Air
2	2.5	20	Air
3	3.90	19.76	Freon
4	3.90	19.76	Air
5	3.19	14.19	Freon
6	3.19	14.19	Air

TABLE OF BASIC TEST DATA 1

RUN	ME	L/D	BETAE	ALFA	PL/PE	PE			PN/PE				PB/PE
NO.						KPA	X/D= 8.10	8.30	8.52	8.74	8.96	9.20	9.42	9.50
5258	2.00	1.0	8.0	0.0	JETOFF	12.66	0.998	1.017	0.758	0.690	0.692	0.707	0.720	0.735
5259	2.00	1.0	8.0	0.0	15.2	12.66	1.004	1.018	0.760	0.689	0.692	0.962	1.308	1.389
5260	2.00	1.0	8.0	0.0	9.2	12.66	1.001	1.016	0.759	0.688	0.691	0.706	1.230	1.318
5261	2.00	1.0	8.0	0.0	6.0	12.66	1.000	1.016	0.758	0.688	0.691	0.705	1.017	1.224
5262	2.00	1.0	8.0	0.0	3.0	12.66	1.000	1.018	0.759	0.690	0.693	0.707	0.736	0.957
5263	2.00	1.0	8.0	0.0	1.0	12.66	0.999	1.017	0.759	0.689	0.693	0.707	0.720	0.605
5264	2.00	1.0	8.0	0.0	JETOFF	12.66	0.998	1.016	0.756	0.688	0.692	0.707	0.718	0.728

TABLE OF BASIC TEST DATA 2

RUN	ME	L/D	BETAE	ALFA	PL/PE	PE			PN/PE				PB/PE
NO.						KPA	X/D= 8.10	8.30	8.52	8.74	8.96	9.20	9.42	9.50
5265	2.00	1.0	8.0	0.0	JETOFF	12.66	0.997	1.015	0.757	0.687	0.691	0.705	0.718	0.724
5268	2.00	1.0	8.0	0.0	9.2	12.66	1.000	1.014	0.757	0.686	0.691	1.205	1.301	1.408
5271	2.00	1.0	8.0	0.0	15.2	12.67	1.000	1.013	0.757	0.685	1.007	1.303	1.280	1.444
5272	2.00	1.0	8.0	0.0	6.0	12.67	0.999	1.015	0.757	0.687	0.690	0.746	1.289	1.369
5273	2.00	1.0	8.0	0.0	3.0	12.67	0.998	1.015	0.757	0.687	0.691	0.705	0.993	1.214
5274	2.00	1.0	8.0	0.0	1.0	12.67	0.998	1.016	0.756	0.687	0.692	0.705	0.721	0.817
5275	2.00	1.0	8.0	0.0	JETOFF	12.67	0.998	1.016	0.756	0.688	0.692	0.705	0.718	0.721

FFA AU 1384 TABLE OF BASIC TEST DATA 3

RUN 5347 ME=2.00 POE= 97.59 KPA PE=12.47 KPA ALPHA=0.0 L/D=1.0 BETAE= 8.0 ML=3.90 THETAL=19.76

T	TO	POI	PN/PE							PB/PE
SEC	C	MPA	X/D=8.10	8.30	8.52	8.74	8.96	9.20	9.42	9.50
0.0	120	1.11					0.690	0.723	0.712	0.650
1.0	206	14.60					0.689	0.723	0.978	1.163
1.9	224	16.60					0.709	0.727	1.201	1.290
2.9	232	16.75	0.989				0.694	0.726	1.220	1.292
3.8	236	16.84		1.003			0.690	0.723	1.216	1.290
4.8	240	16.86					0.689	0.723	1.212	1.286
5.7	243	16.89			0.742		0.689	0.723	1.195	1.284
6.6	246	16.93					0.689	0.723	1.204	1.283
7.6	248	16.93				0.676	0.689	0.723	1.204	1.281
8.5	250	16.96					0.689	0.723	1.201	1.286
9.5	252	16.95					0.689	0.722	1.199	1.277
10.4	253	16.97					0.689	0.722	1.196	1.275

RUN 5348 ME=2.00 POE= 97.60 KPA PE=12.47 KPA ALPHA=0.0 L/D=1.0 BETAE= 8.0 ML=3.90 THETAL=19.76

T	TO	POI	PN/PE							PB/PE
SEC	C	MPA	X/D=8.10	8.30	8.52	8.74	8.96	9.20	9.42	9.50
0.0	253	15.84					0.693	0.726	1.169	1.255
1.0	255	15.93					0.693	0.726	1.167	1.254
1.9	257	15.97					0.714	0.726	1.164	1.253
2.9	258	16.00	0.994				0.698	0.726	1.163	1.252
3.8	259	16.02		1.010			0.694	0.724	1.161	1.251
4.8	260	16.03					0.693	0.725	1.161	1.251
5.7	261	16.05			0.747		0.693	0.726	1.146	1.251
6.6	262	16.06					0.693	0.725	1.157	1.250
7.6	262	16.07				0.680	0.693	0.725	1.158	1.249
8.5	263	16.08					0.693	0.725	1.158	1.247
9.5	263	16.09					0.693	0.725	1.158	1.247
10.4	264	16.10					0.693	0.725	1.158	1.249

FFA AV 1384 TABLE OF BASIC TEST DATA 3 CONT.

RUN 5349 ME=2.00 POE= 97.60 KPA PE=12.47 KPA ALPHA=0.0 L/D=1.0 BETAE= 8.0 ML=3.90 THETAL=19.76

T	TO	POI	PN/PE							PB/PE
SEC	C	MPA	X/D=8.10	8.30	8.52	8.74	8.96	9.20	9.42	9.50
0.0	185	2.37					0.695	0.729	0.706	0.629
0.9	216	5.57					0.695	0.728	0.713	0.773
1.9	226	6.49					0.718	0.728	0.725	0.862
2.8	234	7.06	0.995				0.700	0.728	0.733	0.916
3.8	239	7.42		1.012			0.696	0.726	0.739	0.947
4.7	242	7.69					0.694	0.727	0.744	0.968
5.7	244	7.89			0.748		0.694	0.727	0.747	0.982
6.6	246	8.04					0.694	0.727	0.752	0.992
7.6	247	8.15				0.681	0.694	0.727	0.757	1.000
8.5	248	8.23					0.694	0.727	0.760	1.008
9.5	249	8.29					0.694	0.727	0.762	1.010
10.4	250	8.35					0.694	0.727	0.765	1.013

RUN 5351 ME=2.00 POE= 98.09 KPA PE=12.54 KPA ALPHA=0.0 L/D=1.0 BETAE= 8.0 ML=3.90 THETAL=19.76

T	TO	POI	PN/PE							PB/PE
SEC	C	MPA	X/D=8.10	8.30	8.52	8.74	8.96	9.20	9.42	9.50
0.0	194	8.12					0.692	0.722	0.733	0.952
1.0	212	10.09					0.691	0.722	0.815	1.098
1.9	221	11.34					0.707	0.721	0.936	1.159
2.9	227	12.14	0.988				0.695	0.721	1.019	1.188
3.8	231	12.66		1.002			0.692	0.719	1.059	1.203
4.8	234	12.93					0.691	0.721	1.078	1.209
5.7	236	13.12			0.742		0.691	0.721	1.074	1.212
6.6	238	13.22					0.691	0.721	1.087	1.214
7.6	240	13.30				0.676	0.691	0.721	1.089	1.214
8.5	242	13.40					0.691	0.721	1.090	1.213
9.5	243	13.43					0.691	0.721	1.090	1.214
10.4	245	13.48					0.691	0.721	1.088	1.213

FFA AU 1384 TABLE OF BASIC TEST DATA 3 CONT.

RUN 5352 ME=2.00 POE= 98.11 KPA PE=12.54 KPA ALPHA=0.0 L/D=1.0 BETAE= 8.0 ML=3.90 THETAL=19.76

T	TO	POI	PN/PE							PB/PE
SEC	C	MPA	X/D=8.10	8.30	8.52	8.74	8.96	9.20	9.42	9.50
0.0	183	5.11					0.692	0.721	0.708	0.715
0.9	221	8.78					0.691	0.721	0.735	0.953
1.9	236	10.68					0.707	0.720	0.811	1.086
2.8	243	11.88	0.987				0.695	0.720	0.911	1.141
3.8	247	12.63		1.001			0.691	0.718	0.986	1.168
4.8	250	13.10					0.691	0.719	1.027	1.182
5.7	252	13.41			0.743		0.690	0.719	1.036	1.190
6.6	253	13.60					0.690	0.719	1.055	1.195
7.6	254	13.74				0.676	0.690	0.719	1.064	1.198
8.5	255	13.83					0.690	0.719	1.070	1.199
9.5	256	13.91					0.690	0.719	1.073	1.201
10.4	256	13.98					0.690	0.719	1.077	1.203

RUN 5353 ME=2.00 POE= 98.11 KPA PE=12.54 KPA ALPHA=0.0 L/D=1.0 BETAE= 8.0 ML=3.90 THETAL=19.76

T	TO	POI	PN/PE							PB/PE
SEC	C	MPA	X/D=8.10	8.30	8.52	8.74	8.96	9.20	9.42	9.50
0.0	195	4.94					0.691	0.720	0.703	0.689
0.9	223	6.89					0.691	0.720	0.719	0.848
1.9	234	8.06					0.707	0.720	0.735	0.952
2.8	241	8.77	0.986				0.695	0.720	0.759	1.005
3.8	245	9.23		1.000			0.691	0.717	0.777	1.034
4.7	248	9.60					0.691	0.719	0.790	1.053
5.7	250	9.84			0.742		0.690	0.719	0.798	1.067
6.6	252	10.01					0.690	0.719	0.811	1.075
7.6	252	10.14				0.675	0.690	0.719	0.820	1.082
8.5	253	10.24					0.690	0.719	0.829	1.087
9.5	253	10.32					0.690	0.719	0.834	1.089
10.4	254	10.38					0.690	0.718	0.839	1.092

FFA AU 1384 TABLE OF BASIC TEST DATA 3 CONCLUDED

RUN 5357 ME=2.00 POE=100.14 KPA PE=12.80 KPA ALPHA=0.0 L/D=1.0 BETAE= 8.0 ML=3.90 THETAL=19.76

T	TO	POI	PN/PE							PB/PE
SEC	C	MPA	X/D=8.10	8.30	8.52	8.74	8.96	9.20	9.42	9.50
0.0	165	8.38					0.691	0.720	0.717	0.853
1.0	196	8.48					0.690	0.719	0.739	0.993
1.9	207	8.42					0.704	0.719	0.740	0.991
2.9	213	8.49	0.988				0.693	0.719	0.754	0.984
3.8	218	8.61		1.003			0.690	0.717	0.752	0.985
4.8	221	8.69					0.689	0.718	0.746	0.986
5.7	223	8.73			0.741		0.689	0.719	0.741	0.985
6.6	225	8.76					0.689	0.719	0.740	0.983
7.6	227	8.78				0.674	0.689	0.718	0.738	0.981
8.5	228	8.80					0.689	0.718	0.736	0.982
9.5	230	8.80					0.689	0.718	0.735	0.976
10.4	231	8.80					0.689	0.718	0.735	0.973

FFA AU 1384 TABLE OF BASIC TEST DATA 4

RUN 5366 ME=2.00 POE= 99.13 KPA PE=12.67 KPA ALPHA=0.0 L/D=1.0 BETAE= 8.0 ML=3.90 THETAL=19.76

T	TO	POI	PN/PE							PB/PE
SEC	C	MPA	X/D=8.10	8.30	8.52	8.74	8.96	9.20	9.42	9.50
0.0	191	13.32					0.684	0.724	0.756	0.766
1.0	204	13.45					0.684	0.723	0.752	0.737
1.9	209	13.50					0.701	0.723	0.753	0.793
2.9	212	13.52	0.985				0.688	0.723	0.752	0.794
3.8	213	13.53		1.001			0.684	0.721	0.752	0.795
4.8	214	13.54					0.684	0.722	0.751	0.796
5.7	215	13.55			0.732		0.684	0.723	0.749	0.798
6.6	216	13.55					0.684	0.723	0.750	0.798
7.6	216	13.55				0.672	0.683	0.723	0.750	0.799
8.5	216	13.55					0.683	0.723	0.751	0.804
9.5	216	13.56					0.684	0.722	0.751	0.800
10.4	216	13.56					0.684	0.722	0.751	0.800

RUN 5367 ME=2.00 POE= 99.15 KPA PE=12.67 KPA ALPHA=0.0 L/D=1.0 BETAE= 8.0 ML=3.90 THETAL=19.76

T	TO	POI	PN/PE							PB/PE
SEC	C	MPA	X/D=8.10	3.30	8.52	8.74	8.96	9.20	9.42	9.50
0.0	208	12.74					0.684	0.722	0.752	0.742
1.0	218	12.87					0.684	0.722	0.753	0.771
1.9	222	12.92					0.702	0.722	0.752	0.778
2.9	225	12.94	0.984				0.688	0.722	0.751	0.779
3.8	226	12.95		0.999			0.685	0.719	0.749	0.780
4.8	227	12.96					0.684	0.721	0.749	0.781
5.7	228	12.97			0.733		0.684	0.722	0.747	0.781
6.6	228	12.98					0.684	0.722	0.748	0.782
7.6	229	12.99				0.672	0.684	0.722	0.748	0.782
8.5	229	12.98					0.684	0.722	0.747	0.783
9.5	229	12.99					0.684	0.721	0.748	0.783
10.4	229	12.99					0.684	0.722	0.748	0.784

FFA AU 1384 TABLE OF BASIC TEST DATA 5

RUN 5337 ME=2.00 PDE=101.85 KPA PE=13.02 KPA ALPHA=0.0 L/D=1.0 BETAE= 8.0 ML=3.19 THETAL=14.19

T	TO	POI	PN/PE							PB/PE
SEC	C	MPA	X/D=8.10	8.30	8.52	8.74	8.96	9.20	9.42	9.50
0.0	190	2.31					0.688	0.807	0.995	1.108
1.0	220	7.07					0.687	0.848	1.228	1.304
1.9	226	6.92					0.702	0.786	1.244	1.308
2.9	230	7.01	0.987				0.691	0.789	1.247	1.311
3.8	234	7.15		0.998			0.688	0.816	1.247	1.311
4.8	236	7.35					0.688	0.869	1.247	1.313
5.7	239	7.56			0.743		0.689	0.934	1.239	1.315
6.6	241	7.74					0.689	0.984	1.247	1.317
7.6	243	7.86				0.676	0.690	1.010	1.250	1.318
8.5	244	8.08					0.690	1.033	1.251	1.318
9.5	243	8.27					0.690	1.060	1.252	1.322
10.4	240	8.29					0.691	1.068	1.251	1.322

RUN 5338 ME=2.00 PDE=101.85 KPA PE=13.02 KPA ALPHA=0.0 L/D=1.0 BETAE= 8.0 ML=3.19 THETAL=14.19

T	TO	POI	PN/PE							PB/PE
SEC	C	MPA	X/D=8.10	8.30	8.52	8.74	8.96	9.20	9.42	9.50
0.0	206	10.44					0.698	0.952	0.972	1.103
1.0	220	9.98					0.699	1.184	1.233	1.347
1.9	227	8.26					0.705	1.108	1.256	1.328
2.9	232	7.73	0.996				0.692	1.020	1.252	1.316
3.9	235	7.71		1.004			0.688	0.992	1.250	1.314
4.8	237	7.59					0.688	0.993	1.247	1.312
5.7	238	7.57			0.748		0.688	0.989	1.239	1.311
6.6	239	7.61					0.688	0.995	1.244	1.311
7.6	240	7.66				0.678	0.688	1.003	1.245	1.313
8.5	241	7.71					0.689	1.014	1.245	1.309
9.5	241	7.78					0.689	1.026	1.244	1.311
10.4	242	7.85					0.689	1.033	1.244	1.313

FFA AU 1384 TABLE OF BASIC TEST DATA 5 CONT.

RUN 3340 ME=2.00 POE= 97.92 KPA PE=12.51 KPA ALPHA=0.0 L/D=1.0 BETAE= 8.0 ML=3.19 THETAL=14.19

T	TO	POI	PN/PE							PB/PE
SEC	C	MPA	X/D=8.10	8.30	8.52	8.74	8.96	9.20	9.42	9.50
0.0	219	3.94					0.687	0.721	1.090	1.207
0.9	222	4.03					0.687	0.721	1.098	1.215
1.9	224	4.13					0.710	0.721	1.112	1.224
2.8	226	4.26	0.989				0.693	0.721	1.127	1.232
3.8	229	4.44		1.006			0.690	0.719	1.143	1.241
4.8	231	4.81					0.689	0.721	1.167	1.257
5.7	232	5.26			0.745		0.690	0.723	1.178	1.273
6.6	234	7.11					0.689	0.731	1.227	1.304
7.6	229	7.27				0.678	0.689	0.967	1.245	1.316
8.5	225	6.46					0.690	0.871	1.242	1.307
9.5	223	5.65					0.690	0.766	1.228	1.295
10.4	223	5.08					0.690	0.732	1.205	1.277

RUN 3343 ME=2.00 POE= 97.47 KPA PE=12.46 KPA ALPHA=0.0 L/D=1.0 BETAE= 8.0 ML=3.19 THETAL=14.19

T	TO	POI	PN/PE							PB/PE
SEC	C	MPA	X/D=8.10	8.30	8.52	8.74	8.96	9.20	9.42	9.50
0.0	117	0.96					0.694	0.726	0.709	0.707
0.9	193	3.89					0.694	0.726	1.039	1.192
1.9	206	3.77					0.710	0.726	1.084	1.207
2.8	211	3.59	0.992				0.698	0.726	1.046	1.190
3.8	215	3.59		1.008			0.695	0.724	1.022	1.184
4.7	218	3.65					0.694	0.725	1.029	1.190
5.7	221	3.77			0.745		0.694	0.725	1.041	1.201
6.6	223	3.68					0.694	0.725	1.072	1.210
7.6	226	4.01				0.681	0.694	0.725	1.099	1.220
8.5	227	4.15					0.694	0.725	1.119	1.228
9.5	229	4.31					0.695	0.725	1.138	1.240
10.4	23	0.01					0.690	0.721	0.701	0.713

FFA AU 1384

TABLE OF BASIC TEST DATA 5 CONCLUDED

RUN 5344 ME=2.00 POE= 97.47 KPA PE=12.46 KPA ALPHA=0.0 L/D=1.0 BETAE= 8.0 ML=3.19 THETAL=14.19

T	TO	POI	PN/PE							PB/PE
SEC	C	MPA	X/D=8.10	8.30	8.52	8.74	8.96	9.20	9.42	9.50
0.0	206	2.40					0.696	0.727	0.780	1.031
0.9	210	2.35					0.696	0.727	0.769	1.021
1.9	212	2.30					0.712	0.727	0.760	1.010
2.8	214	2.25	0.993				0.700	0.727	0.754	1.000
3.8	216	2.19		1.010			0.696	0.724	0.750	0.990
4.7	217	2.13					0.696	0.726	0.746	0.979
5.7	218	2.10			0.746		0.696	0.726	0.742	0.971
6.6	219	2.06					0.695	0.726	0.741	0.965
7.6	220	2.01				0.682	0.696	0.726	0.739	0.956
8.5	221	1.96					0.696	0.725	0.736	0.950
9.5	221	1.92					0.696	0.725	0.734	0.937
10.4	221	1.83					0.696	0.725	0.732	0.922

FFA AU 1384 TABLE OF BASIC TEST DATA 6

RUN 5368 ME=2.00 POE= 99.20 KPA PE=12.68 KPA ALPHA=0.0 L/D=1.0 BETAE= 8.0 RL=3.19 THETAL=14.19

T	TO	POI	PN/PE							PB/PE
SEC	C	MPA	X/D=8.10	8.30	8.52	8.74	8.96	9.20	9.42	9.50
0.0	152	1.96					0.690	0.720	0.735	0.600
1.0	168	2.03					0.689	0.720	0.736	0.604
1.9	176	2.05					0.705	0.720	0.735	0.606
2.9	181	2.07	0.985				0.693	0.719	0.733	0.609
3.8	185	2.08		1.001			0.690	0.717	0.729	0.610
4.8	189	2.10					0.689	0.719	0.727	0.612
5.7	192	2.11			0.738		0.689	0.719	0.725	0.614
6.6	194	2.12					0.689	0.719	0.724	0.615
7.6	197	2.12				0.675	0.689	0.719	0.724	0.616
8.5	199	2.13					0.689	0.719	0.723	0.622
9.5	200	2.14					0.689	0.719	0.723	0.620
10.4	202	2.14					0.689	0.719	0.723	0.620

RUN 5369 ME=2.00 POE= 99.20 KPA PE=12.68 KPA ALPHA=0.0 L/D=1.0 BETAE= 8.0 RL=3.19 THETAL=14.19

T	TO	POI	PN/PE							PB/PE
SEC	C	MPA	X/D=8.10	8.30	8.52	8.74	8.96	9.20	9.42	9.50
0.0	209	3.62					0.690	0.719	0.737	0.723
0.9	217	3.69					0.689	0.719	0.730	0.742
1.9	221	3.72					0.706	0.719	0.727	0.748
2.8	223	3.75	0.985				0.693	0.719	0.725	0.751
3.8	225	3.76		1.000			0.689	0.716	0.725	0.753
4.7	226	3.77					0.689	0.718	0.724	0.755
5.7	227	3.78			0.739		0.689	0.718	0.724	0.756
6.6	227	3.79					0.689	0.718	0.724	0.757
7.6	228	3.79				0.675	0.689	0.718	0.724	0.759
8.5	228	3.79					0.689	0.718	0.724	0.760
9.5	228	3.80					0.689	0.718	0.724	0.763
10.4	228	3.80					0.689	0.718	0.724	0.763

FFA AU 1384 TABLE OF BASIC TEST DATA 6 CONCLUDED

RUN 5370 ME=2.00 POE= 99.20 KPA PE=12.68 KPA ALPHA=0.0 L/D=1.0 BETAE= 8.0 ML=3.19 THETAL=14.19

T	TO	POI	PN/PE							PB/PE
SEC	C	MPA	X/D=8.10	8.30	8.52	8.74	8.96	9.20	9.42	9.50
0.0	226	5.84					0.691	0.719	0.736	0.840
1.0	230	5.95					0.689	0.718	0.738	0.885
1.9	233	6.01					0.706	0.718	0.748	0.897
2.9	235	6.04	0.986				0.693	0.718	0.744	0.901
3.8	236	6.06		0.998			0.689	0.715	0.758	0.903
4.8	236	6.07					0.688	0.717	0.753	0.905
5.7	237	6.09			0.741		0.688	0.717	0.748	0.906
6.6	237	6.10					0.688	0.717	0.746	0.907
7.6	237	6.10				0.675	0.689	0.717	0.744	0.908
8.5	237	6.11					0.689	0.717	0.744	0.915
9.5	237	6.12					0.689	0.717	0.744	0.911
10.4	237	6.12					0.689	0.717	0.744	0.911


DA
FILM